DETERMINATION OF PATIENT-SPECIFIC FUNCTIONAL AXES THROUGH TWO-LEVEL OPTIMIZATION

By

JEFFREY A. REINBOLT

A THESIS PRESENTED TO THE GRADUATE SCHOOL
OF THE UNIVERSITY OF FLORIDA IN PARTIAL FULFILLMENT
OF THE REQUIREMENTS FOR THE DEGREE OF
MASTER OF SCIENCE

UNIVERSITY OF FLORIDA

2003

This thesis is dedicated to my loving wife, Karen.

ACKNOWLEDGMENTS

I sincerely thank Dr. B. J. Fregly for his support and leadership throughout our research endeavors; moreover, I truly recognize the value of his honest, straightforward, and experience-based advice. My life has been genuinely influenced by Dr. Fregly's expectations, confidence, and trust in me.

I also extend gratitude to Dr. Raphael Haftka and Dr. Roger Tran-Son-Tay for their dedication, knowledge, and instruction in the classroom. For these reasons, each was selected to serve on my supervisory committee. I express thanks to both individuals for their time, contribution, and fulfillment of their committee responsibilities.

I recognize Jaco for his assistance, collaboration, and suggestions. His dedication and professionalism have allowed my graduate work to be both enjoyable and rewarding.

I collectively show appreciation for my family and friends. Unconditionally, they have provided me with encouragement, support, and interest in my graduate studies and research activities.

My wife, Karen, has done more for me than any person could desire. On several occasions, she has taken a leap of faith with me; more importantly, she has been directly beside me. Words or actions cannot adequately express my gratefulness and adoration toward her. I honestly hope that I can provide her as much as she has given to me.

I thank God for my excellent health, inquisitive mind, strong faith, valuable experiences, encouraging teachers, loving family, supportive friends, and wonderful wife.

TABLE OF CONTENTS

LIST OF TABLES

LIST OF FIGURES

Abstract of Thesis Presented to the Graduate School
of the University of Florida in Partial Fulfillment of the
Requirements for the Degree of Master of Science

DETERMINATION OF PATIENT-SPECIFIC FUNCTIONAL AXES
THROUGH TWO-LEVEL OPTIMIZATION

By

Jeffrey A. Reinbolt

August 2003

Chair: Benjamin J. Fregly
Major Department: Biomedical Engineering

An innovative patient-specific dynamic model would be useful for evaluating and enhancing corrective surgical procedures. This thesis presents a nested (or two-level) system identification optimization approach to determine patient-specific model parameters that best fit a three-dimensional (3D), 18 degree-of-freedom (DOF) lower-body model to an individual's movement data.

The whole body was modeled as a 3D, 14 segment, 27 DOF linkage joined by a set of gimbal, universal, and pin joints. For a given set of model parameters, the inner-level optimization uses a nonlinear least squares algorithm that adjusts each generalized coordinate of the lower-body model to minimize 3D marker coordinate errors between the model and motion data for each time instance. The outer-level optimization implements a parallel particle swarm algorithm that modifies each model parameter to minimize the sum of the squares of 3D marker coordinate errors computed by the inner-level optimization throughout all time instances (or the entire motion).

At the termination of each two-level optimization using synthetic marker data without noise, original marker trajectories were precisely recovered to within an arbitrarily tight tolerance (on the order of 1e-13 cm) using double precision computations. At the termination of each two-level optimization using synthetic marker data with noise representative of skin and soft tissue movement artifacts, the mean marker distance error for each joint complex was as follows: ankle = 0.51 $\pm$ 0.23 cm; knee = 0.39 $\pm$ 0.15 cm; and hip = 0.47 $\pm$ 0.20 cm. Mean marker distance errors are approximately one-half of the 1 cm maximum amplitude specified for the noise model. At the termination of each two-level optimization using experimental marker data from one subject, the mean marker distance error for each joint complex was less than or equal to the following: ankle = 0.38 $\pm$ 0.19 cm; knee = 0.55 $\pm$ 0.27 cm; and hip = 0.36 $\pm$ 0.20 cm. Experimental mean marker distance error results are comparable to the results of the synthetic data with noise.

The two-level optimization method effectively determines patient-specific model parameters defining a 3D lower-extremity model that is well suited to a particular subject. When compared to previous values in the literature, experimental results show reasonable agreement and demonstrate the necessity for the new approach. By minimizing fitness errors between the patient-specific model and experimental motion data, the resulting kinematic model provides an accurate foundation for future dynamic analyses and optimizations.

CHAPTER 1
INTRODUCTION

Arthritis: The Nation's Leading Cause of Disability

In 1997, the Centers for Disease Control and Prevention (CDC) reported that 43 million (or 1 in 6) Americans suffered with arthritis. A 2002 CDC study showed that 70 million (a 63% increase in 5 years; or 1 in 3) Americans have arthritis (CDC, 2003). Approximately two-thirds of individuals with arthritis are under 65 years old. As the population ages, the number of people with arthritis is likely to increase significantly. The most common forms of arthritis are osteoarthritis, rheumatoid arthritis, fibromyalgia, and gout. Osteoarthritis of the knee joint accounts for roughly 30% ($25 billion) of the $82 billion total arthritis costs per year in the United States.

Knee osteoarthritis symptoms of pain and dysfunction are the primary reasons for total knee replacement (TKR). This procedure involves a resurfacing of bones surrounding the knee joint. The end of the femur is removed and covered with a metal implant. The end of the tibia is removed and substituted by a plastic implant. Smooth metal and plastic articulation replaces the irregular and painful arthritic surfaces. Approximately 100,000 Medicare patients alone endure TKR procedures each year (Heck et al., 1998). Hospital charges for unilateral TKR are more than $30,000 and the cost of bilateral TKR is over $50,000 (Lane et al., 1997).

An alternative to TKR is a more conservative (both economically and surgically) corrective procedure known as high tibial osteotomy (HTO). By changing the frontal plane alignment of the tibia with a wedge of bone, a HTO shifts the weight-bearing axis

of the leg, and thus the mechanical stresses, from the diseased portion to the healthy section of the knee compartment. By transferring the location of mechanical stresses, the degenerative disease process may be slowed or possibly reversed. The advantages of HTO are appealing to younger and active patients who receive recommendations to avoid TKR.

Need for Accurate Patient-Specific Models

Innovative patient-specific models and simulations would be valuable for addressing problems in orthopedics and sports medicine, as well as for evaluating and enhancing corrective surgical procedures (Arnold et al., 2000; Arnold and Delp, 2001; Chao et al., 1993; Chao and Sim, 1995; Delp et al., 1998; Delp et al., 1996; Delp et al., 1990; Pandy, 2001). For example, a patient-specific dynamic model may be useful for planning intended surgical parameters and predicting the outcome of HTO.

The main motivation for developing a patient-specific computational model and a two-level optimization method to enhance the lower-extremity portion is to predict the post-surgery peak knee adduction moment in HTO patients. Conventional surgical planning techniques for HTO involve choosing the amount of necessary tibial angulation from standing radiographs (or x-rays). Unfortunately, alignment correction estimates from static x-rays do not accurately predict long-term clinical outcome after HTO (Andriacchi, 1994; Tetsworth and Paley, 1994). Researchers have identified the peak external knee adduction moment as an indicator of clinical outcome while investigating the gait of HTO patients (Andriacchi, 1994; Bryan et al., 1997; Hurwitz et al., 1998; Prodromos et al., 1985; Wang et al., 1990). Currently, no movement simulations (or other methods for that matter) allow surgeons to choose HTO surgical parameters to achieve a chosen post-surgery knee adduction moment.

Movement simulations consist of models involving skeletal structure, muscle paths, musculotendon actuation, muscle excitation-contraction coupling, and a motor task goal (Pandy, 2001). Development of an accurate inverse dynamic model of the skeletal structure is a significant first step toward creating a predictive patient-specific forward dynamic model to perform movement simulations.

The precision of dynamic analyses is fundamentally associated with the accuracy of kinematic model parameters such as segment lengths, joint positions, and joint orientations (Andriacchi and Strickland, 1985; Challis and Kerwin, 1996; Cappozzo et al., 1975; Davis, 1992; Holden and Stanhope, 1998; Holden and Stanhope, 2000; Stagni et al., 2000). Understandably, a model constructed of rigid links within a multi-link chain and simple mechanical approximations of joints will not precisely match the human anatomy and kinematics. The model should provide the best possible agreement to experimental motion data within the bounds of the joint models selected (Sommer and Miller, 1980).

Benefits of Two-Level Optimization

This thesis presents a nested (or two-level) system identification optimization approach to determine patient-specific joint parameters that best fit a three-dimensional (3D), 18 degree-of-freedom (DOF) lower-body model to an individual's movement data. The two-level technique combines the advantages of using optimization to determine both the position of model segments from marker data and the anatomical joint axes linking adjacent segments. By formulating a two-level objective function to minimize marker coordinate errors, the resulting optimum model more accurately represents experimental marker data (or a specific patient and his or her motion) when compared to a nominal model defined by joint axes prediction methods.

CHAPTER 2
BACKGROUND

Motion Capture

Motion capture is the use of external devices to capture the movement of a real object. One type of motion-capture technology is based on a passive optical technique. Passive refers to markers, which are simply spheres covered in reflective tape, placed on the object. Optical refers to the technology used to provide 3D data, which involves high-speed, high-resolution video cameras. By placing passive markers on an object, special hardware records the position of those markers in time and it generates a set of motion data (or marker data).

Often motion capture is used to create synthetic actors by capturing the motions of real humans. Special effects companies have used this technique to produce incredibly realistic animations in movies such as Star Wars Episode I & II, Titanic, Batman, and Terminator 2.

Biomechanical Models

Researchers use motion-capture technology to construct biomechanical models of the human structure. The position of external markers may be used to estimate the position of internal landmarks such as joint centers. The markers also enable the creation of individual segment reference frames that define the position and orientation of each body segment within a Newtonian laboratory reference frame. Marker data collected from an individual are used to prescribe the motion of the biomechanical model.

Kinematics and Dynamics

Human kinematics is the study of the positions, angles, velocities, and accelerations of body segments and joints during motion. With kinematic data and mass-distribution data, one can study the forces and torques required to produce the recorded motion data. Errors between the biomechanical model and the recorded motion data will inevitably propagate to errors in the force and torque results of dynamic analyses.

Optimization

Optimization involves searching for the minimum or maximum of an objective function by adjusting a set of design variables. For example, the objective function may be the errors between the biomechanical model and the recorded motion data. These errors are a function of the model's generalized coordinates and the model's kinematic parameters such as segment lengths, joint positions, and joint orientations. Optimization may be used to modify the design variables of the model to minimize the overall fitness errors and identify a structure that matches the experimental data very well.

Limitations of Previous Methods

The literature contains a number of examples that use techniques, with or without optimization, to assist in the development of subject-specific joint models within a larger computational model. Several authors have presented methodologies to predict joint locations and orientations from external landmarks without using optimization (Bell et al., 1990; Inman, 1976; Vaughan et al., 1992). However, a regression model based solely upon population studies may not accurately portray an individual patient. Another study demonstrated an optimization method to determine the position and orientation of a 3 link, 6 DOF model by minimizing the distances between model-determined and experimental marker positions (Lu and O'Connor, 1999). A model optimally positioned

without adjusting its joint parameters may not properly correspond to a certain patient. Earlier studies described optimization methods to determine a set of model parameters for a 3D, 2 DOF model by decreasing the error between the motion of the model and experimental data (Sommer and Miller, 1980; Bogert et al., 1994). A model defined by optimal joint parameters without optimizing its segment positions may not accurately describe the motion of a patient within the bounds of the chosen joint approximations.

CHAPTER 3
METHODS

Parametric Model Structure

A generic, parametric 3D full-body kinematic model was constructed with Autolev™ (Online Dynamics, Inc., Sunnyvale, CA) as a 14 segment, 27 DOF linkage joined by a set of gimbal, universal, and pin joints (Figure 3-1, Table 3-1). Comparable to Pandy's (2001) model structure, 3 translational degrees of freedom (DOFs) (q_1, q_2, and q_3) and 3 rotational DOFs (q_4, q_5, and q_6) express the movement of the pelvis in 3D space and the remaining 13 body segments comprise four open chains branching from the pelvis segment. The locations and orientations of the joints within corresponding body segments are described by 98 patient-specific model parameters. In other words, the patient-specific model parameters designate the geometry of the model containing the following joints types: 3 DOF hip, 1 DOF knee, 2 DOF ankle, 3 DOF back, 2 DOF shoulder, and 1 DOF elbow. Each joint is defined in two adjacent body segments and provides a mechanical approximation connecting those segments (Figure 3-2). For example, the knee joint axis is simultaneously established in the femur coordinate system and the tibia coordinate system.

A modified version of the Cleveland Clinic marker set (Figure 3-3) and a static motion-capture trial is used to create segment coordinate systems and define static and dynamic marker locations in these coordinate systems. Institutional review board approval and proper informed consent were obtained before human involvement in the experiments. The marker data collection system was a HiRes Expert Vision System

(Motion Analysis Corp., Santa Rosa, CA), including six HSC-180 cameras, EVa 5.11 software, and two AMTI force plates (Advanced Management Technology, Inc., Arlington, VA). Marker data were collected at 180 Hz during 3 seconds for static trials and 6 seconds for individual joint trials. The raw data were filtered using a fourth-order, zero phase-shift, low pass Butterworth Filter with a cutoff frequency set at 6 Hz.

Hip Joint

There are 6 translational model parameters that must be adjusted to establish a functional hip joint center for a particular patient (Figure 3-4, Table 3-2). Markers placed over the left anterior superior iliac spine (ASIS), right ASIS, and superior sacrum define the pelvis segment coordinate system. From percentages of the inter-ASIS distance, a predicted (or nominal) hip joint center location within the pelvis segment is 19.3% posterior (p_1), 30.4% inferior (p_2), and 35.9% medial-lateral (p_3) (Bell et al., 1990). This nominal hip joint center is the origin of the femur coordinate system, which is subsequently defined by markers placed over the medial and lateral femoral epicondyles. An additional 3 translational model parameters (p_4, p_5, and p_6), described in the femur coordinate system, complete the structure of the nominal hip joint center.

Given the physical hip joint center is located within the pelvic region lateral to the midsagittal plane, a cube with side lengths equal to 75% of the inter-ASIS distance and its anterior-superior-medial vertex positioned at the midpoint of the inter-ASIS line provides the geometric constraints for the optimization of each model parameter (Figure 3-5, Table A-1, Table B-1).

Knee Joint

There are 9 model parameters (5 translational and 4 rotational) that must be tailored to identify a patient-specific functional knee joint axis (Figure 3-6, Table 3-3). The

femoral transepicondylar axis is a good approximation of a fixed knee joint axis (Churchill et al., 1998). The line (or nominal) knee joint axis, connecting the medial and lateral knee markers is defined in the femur and tibia coordinate systems (Vaughan et al., 1992). Given the line passes through the midsagittal plane (x-y plane) of the femur segment, the nominal knee joint axis is positioned within the femur via 2 translational model parameters (p_5 and p_6) and 2 rotational model parameters (p_1 and p_2). The tibia coordinate system originates at the midpoint of the knee markers and is defined by additional markers located on the medial and lateral malleoli. The distal description of the nominal knee joint axis is comprised of 3 translational model parameters (p_7, p_8, and p_9) and 2 rotational model parameters (p_3 and p_4) in the tibia segment.

Given the anatomical knee joint DOFs are situated within the articular capsule, a cube with side lengths equal to the distance between knee markers and its center located at the midpoint of the nominal knee joint axis provides the geometric constraints for the optimization of each translational model parameter. The rotational model parameters are constrained within a circular cone defined by the 360° revolution of the nominal knee joint axis perturbed by $\pm$ 30° (Figure 3-5, Table A-2, Table B-2).

It is not a trivial notion to eliminate a potential medial-lateral translational model parameter in the femur segment. This model parameter is considered redundant, as the knee joint axis passes through the midsagittal plane of the femur, and its inclusion may lead to possible optimization convergence problems, similar to the redundant ankle model parameter discussion of Bogert et al. (1994). By including redundant model parameters, there are an infinite number of optimum solutions within the constraints of corresponding superfluous model parameters.

Ankle Joint

There are 12 patient-specific model parameters (7 translational and 5 rotational) that must be customized to determine a pair of patient-specific functional ankle joint axes (Figure 3-7, Table 3-4). Comparable to Bogert et al. (1994), the talocrural and subtalar joints connect the tibia, talus, and foot segments. Within the tibia segment, 3 translational model parameters (p_6, p_7, and p_8) and 2 rotational model parameters (p_1 and p_2) position the nominal talocrural joint axis. The talus origin corresponds to the talocrural joint center; therefore, it is not necessary to prescribe model parameters defining the talocrural joint axis in the talus segment. The talus coordinate system is created where the y-axis extends along the line perpendicular to both the talocrural joint axis and the subtalar joint axis. The heel and toe markers, in combination with the tibia y-axis, define the foot coordinate system. There are 3 translational model parameters (p_{10}, p_{11}, and p_{12}) and 2 rotational model parameters (p_4 and p_5) (Inman, 1976) that place the nominal subtalar joint axis in the foot coordinate system.

Given the anatomical ankle joint DOFs are found within the articular capsule, a cube with side lengths equal to the distance between ankle markers and its center located at the midpoint of the nominal talocrural joint axis provides the geometric constraints for the optimization of each translational model parameter. The rotational model parameters of the talocrural joint axis are restricted within a circular cone defined by the 360° revolution of the nominal talocrural joint axis varied by $\pm$ 30°. The rotational model parameters of the subtalar joint axis are confined within a circular cone defined by the 360° revolution of the nominal subtalar joint axis altered by $\pm$ 30° (Figure 3-5, Table A-3, Table B-3).

Two-Level Optimization Approach

Why Two Levels of Optimization Are Necessary

Optimization may be used to identify a system (or determine patient-specific joint parameters) that best fit a 3D, 18 DOF lower-body model to an individual's movement data. One level of optimization is necessary to establish the model's geometry. Given a defined model, another level of optimization is required to position and orientate the model's body segments. By formulating a two-level objective function to minimize 3D marker coordinate errors, the two-level optimization results describe a lower-body model that accurately represents experimental data.

Inner-Level Optimization

Given marker trajectory data, m_d, and a constant set of patient-specific model parameters, p, the inner-level optimization (Figure 3-8, inner boxes) minimizes the 3D marker coordinate errors, e_c, between the model markers, m_m, and the marker movement data, m_d, (Equation 3-1) using a nonlinear least squares algorithm that adjusts the generalized coordinates, q, of the model at each instance in time, t, (Figure 3-9), similar to Lu and O'Connor (1999). In other words, the pose of the model is revised to match the marker movement data at each time frame of the entire motion.

$$\min \; e_c(q, p, t) \;=\; m_d(t) \;-\; m_m(q, p, t) \tag{3-1}$$

At the first time instance, the algorithm is seeded with exact values for the 6 generalized coordinates of the pelvis, since the marker locations directly identify the position and orientation of the pelvis coordinate system, and all remaining generalized coordinates are seeded with values equal to zero. Given the joint motion is continuous, each optimal generalized coordinate solution, including the pelvis generalized

coordinates, at one time instance is used as the algorithm's seed for the next time instance. Matlab 6.1 (The MathWorks, Inc., Natick, MA), in conjunction with the Matlab Optimization Toolbox and Matlab C/C++ Compiler, was used to develop the inner-level optimization program.

Outer-Level Optimization

The outer-level global optimization (Figure 3-8, outer boxes) minimizes the sum of the squares, e_{ss}, of the 3D marker coordinate errors, e_c, (Equation 3-1) computed by the inner-level algorithm throughout all time instances, n, (Equation 3-2) by modifying the patient-specific model parameters, p. In other words, the geometric structure of the model is varied to best fit the marker movement data for the entire motion.

$$\min \quad e_{ss}(q, p, n) \quad = \quad \sum_{t=1}^{n} \left[e_c(q, p, t)\right]^T \left[e_c(q, p, t)\right] \tag{3-2}$$

The outer-level optimization is adapted from the population-based Particle Swarm Optimizer (PSO) (Kennedy and Eberhart, 1995). The PSO algorithm was chosen over gradient-based optimizers for its suitability to be parallelized and its ability to solve global optimization problems. It is particularly effective in the determination of joint positions and orientations of biomechanical systems (Schutte et al., 2003). The work of Schutte et al. (2003) contrasted the PSO to a gradient-based optimizer (i.e., Broyden-Fletcher-Goldfarb-Shanno) that is commonly used in system identification problems involving biomechanical models. The PSO very reliably converged to the global minimum and it was insensitive to both design variable scaling and initial seeds (Schutte et al., 2003).

To manage computational requirements, the outer-level optimization uses a parallel version of the PSO operating on a cluster of 20 Linux-based 1.33 GHz Athlon PC's on a

100 Mbps switched Fast Ethernet network. Each machine is separately seeded with a random set of initial patient-specific model parameter values. The outer-level optimization program was implemented in C on the Linux operating system with the Message Passing Interface (MPI) parallel computation libraries.

Two-Level Optimization Evaluation

Synthetic Marker Data without Noise

To evaluate the ability of the two-level optimization approach (Figure 3-10) to calibrate the generic, parametric kinematic model, synthetic movement data was generated for the ankle, knee, and hip joints based on estimated *in vivo* model parameters and experimental movement data. For each generated motion, the distal segment moved within the physiological range of motion and exercised each DOF for the joint. There were 50 time frames and approximately 3.5 cycles of a circumductive hip motion consisting of concurrent flexion-extension and abduction-adduction. Flexion-extension comprised 50 time frames and roughly 4 cycles of knee motion. The ankle motion involved 50 time frames and nearly 2.75 cycles of circumduction of the toe tip, where plantarflexion-dorsiflexion and inversion-eversion occurred simultaneously. The ability of the two-level optimization to recover the original model parameters used when generating the synthetic motions was assessed.

Synthetic Marker Data with Noise

To evaluate the ability of the two-level optimization method (Figure 3-10) to calibrate the generic kinematic model to a synthetic patient, skin movement artifacts were introduced into the synthetic movement data for the ankle, knee, and hip joints. The relative movement between skin and underlying bone occurs in a continuous rather than a random fashion (Cappozzo et al., 1993). Comparable to the simulated skin movement

artifacts of Lu and O'Connor (1999), a continuous numerical noise model of the form $A\sin(\omega t+\varphi)$ was used and the equation variables were randomly generated within the following bounds: amplitude ($0 \le A \le 1$ cm), frequency ($0 \le \omega \le 25$ rad/s), and phase angle ($0 \le \varphi \le 2\pi$) (Chéze et al., 1995). Noise was separately generated for each 3D coordinate of the marker trajectories. Again, the two-level optimization was tested for its ability to reproduce the original model parameters.

Experimental Marker Data

To verify the ability of the two-level optimization technique (Figure 3-10) to calibrate the generic kinematic model to a particular patient, multi-cycle experimental marker trajectory data was collected from one subject. For each joint motion, the distal segment moved within the physiological range of motion and exercised each DOF for the joint. Analogous to Bogert et al. (1994), the original data were resampled non-equidistantly to eliminate weighting the data set with many data points occurring during acceleration and deceleration at the limits of the range of motion. In other words, regardless of changes in velocity during joint movements, the data was equally distributed over the entire joint range of motion. The time frames of original tracked marker data sets (right hip = 1015, right knee = 840, and right ankle = 707) were reduced to 50 time frames. The resampled data allowed a fixed amount of marker movement between frames to arrive at the number of time frames chosen, given that 50 time frames is analogous to Lu and O'Connor (1999). There were nearly 2 cycles of flexion-extension and abduction-adduction involved in the hip motion. Similar to Leardini et al. (1999), internal-external rotation of the hip was avoided to reduce the effects of skin and soft tissue movement artifacts. Approximately 2 cycles of knee

motion included flexion-extension. Simultaneous plantarflexion-dorsiflexion and inversion-eversion comprised roughly 2 cycles of ankle motion. Without knowledge of original model parameters, the marker coordinate errors are the only means of measuring the effectiveness of the two-level optimization.

To verify the ability of the two-level optimization procedure (Figure 3-10) to calibrate the generic kinematic model to a particular patient using a smaller portion of the joint motion cycle, the resampled multi-cycle experimental marker trajectory data described above was divided into the first and second halves of the individual hip, knee, and ankle joint motion cycles. The number of time frames comprising each one-half-cycle of the joint motion was as follows: ankle = 13, knee = 13, and hip = 19. Again, the two-level optimization was tested for its ability to reduce the marker coordinate errors and obtain an optimal set of model parameters.

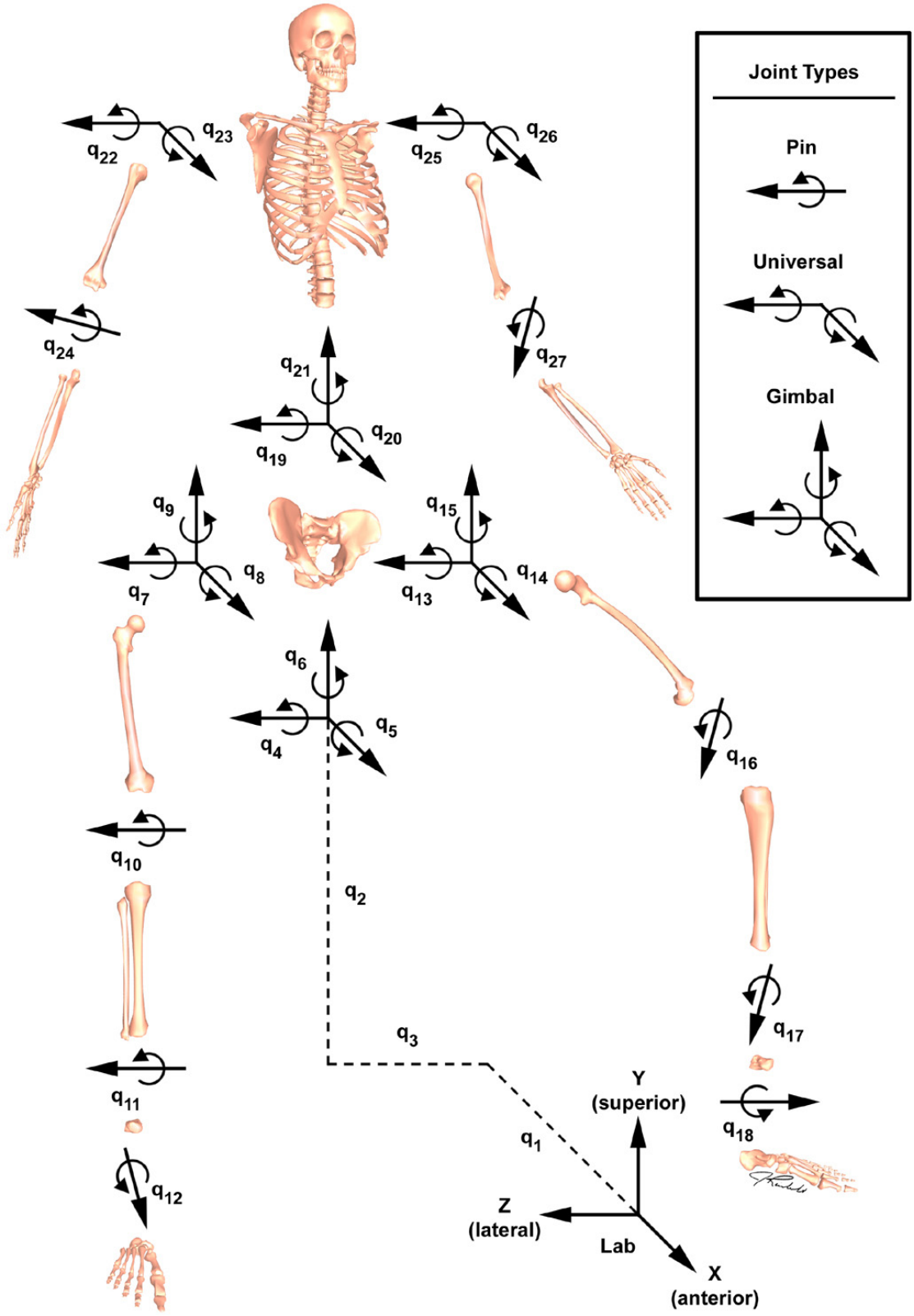

Figure 3-1. The 3D, 14 segment, 27 DOF full-body kinematic model linkage joined by a set of gimbal, universal, and pin joints.

Table 3-1. Model degrees of freedom.

DOF	Description
q_1	Pelvis anterior-posterior position
q_2	Pelvis superior-inferior position
q_3	Pelvis medial-lateral position
q_4	Pelvis anterior-posterior tilt angle
q_5	Pelvis elevation-depression angle
q_6	Pelvis internal-external rotation angle
q_7	Right hip flexion-extension angle
q_8	Right hip adduction-abduction angle
q_9	Right hip internal-external rotation angle
q_{10}	Right knee flexion-extension angle
q_{11}	Right ankle plantarflexion-dorsiflexion angle
q_{12}	Right ankle inversion-eversion angle
q_{13}	Left hip flexion-extension angle
q_{14}	Left hip adduction-abduction angle
q_{15}	Left hip internal-external rotation angle
q_{16}	Left knee flexion-extension angle
q_{17}	Left ankle plantarflexion-dorsiflexion angle
q_{18}	Left ankle inversion-eversion angle
q_{19}	Trunk anterior-posterior tilt angle
q_{20}	Trunk elevation-depression angle
q_{21}	Trunk internal-external rotation angle
q_{22}	Right shoulder flexion-extension angle
q_{23}	Right shoulder adduction-abduction angle
q_{24}	Right elbow flexion angle
q_{25}	Left shoulder flexion-extension angle
q_{26}	Left shoulder adduction-abduction angle
q_{27}	Left elbow flexion angle

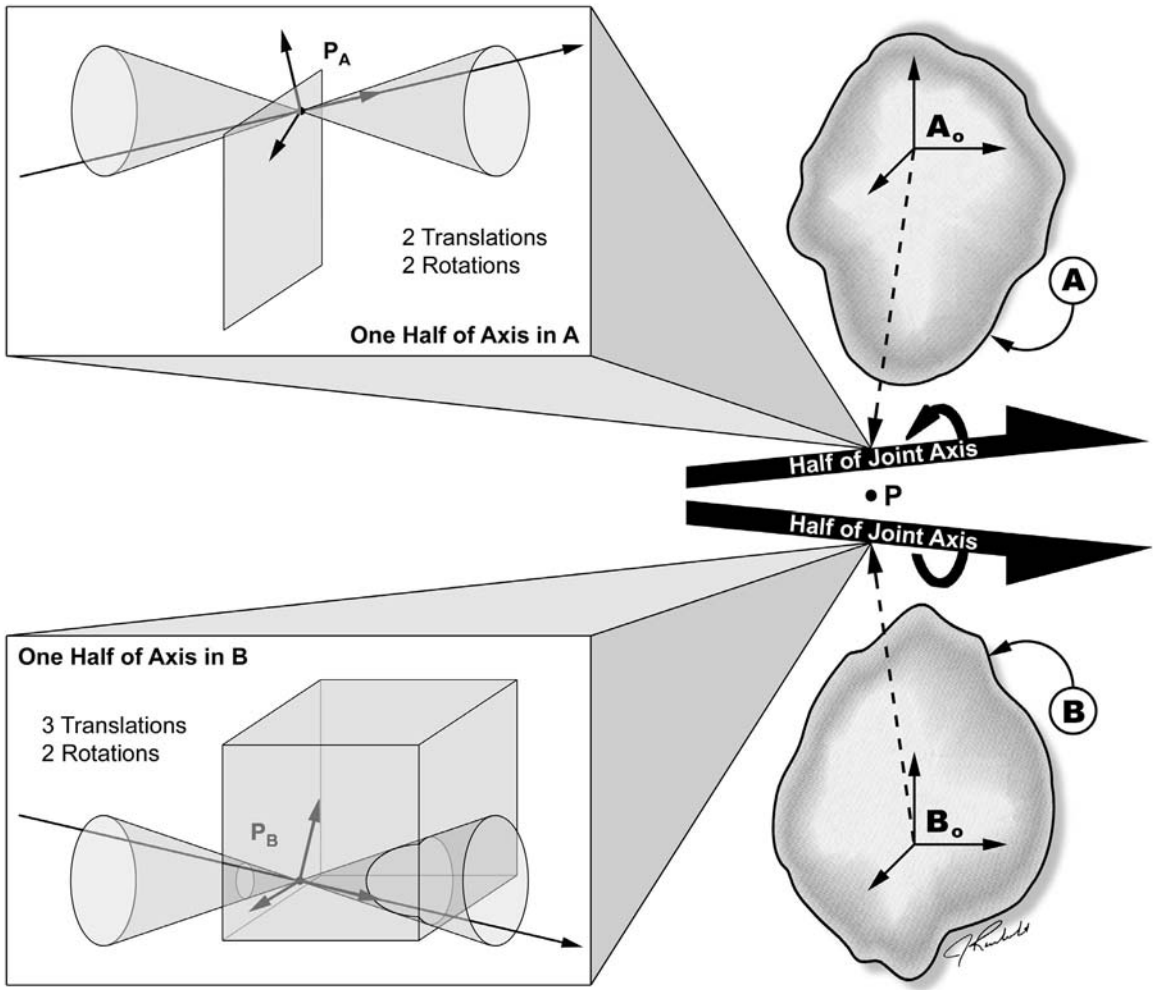

Figure 3-2. A 1 DOF joint axis simultaneously defined in two adjacent body segments and the geometric constraints on the optimization of each of the 9 model parameters.

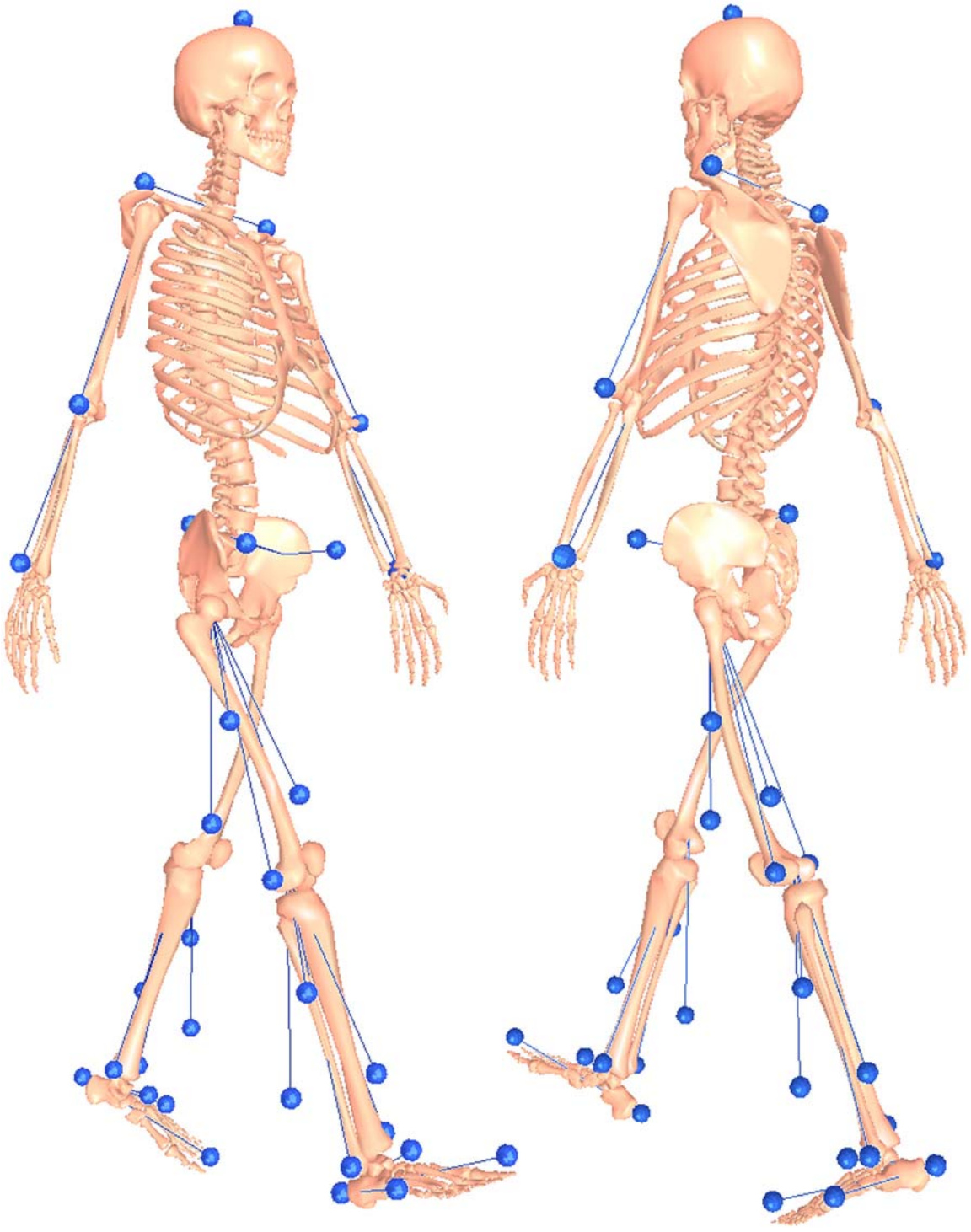

Figure 3-3. Modified Cleveland Clinic marker set used during static and dynamic motion-capture trials. Note: the background femur and knee markers have been omitted for clarity and the medial and lateral markers for the knee and ankle are removed following the static trial.

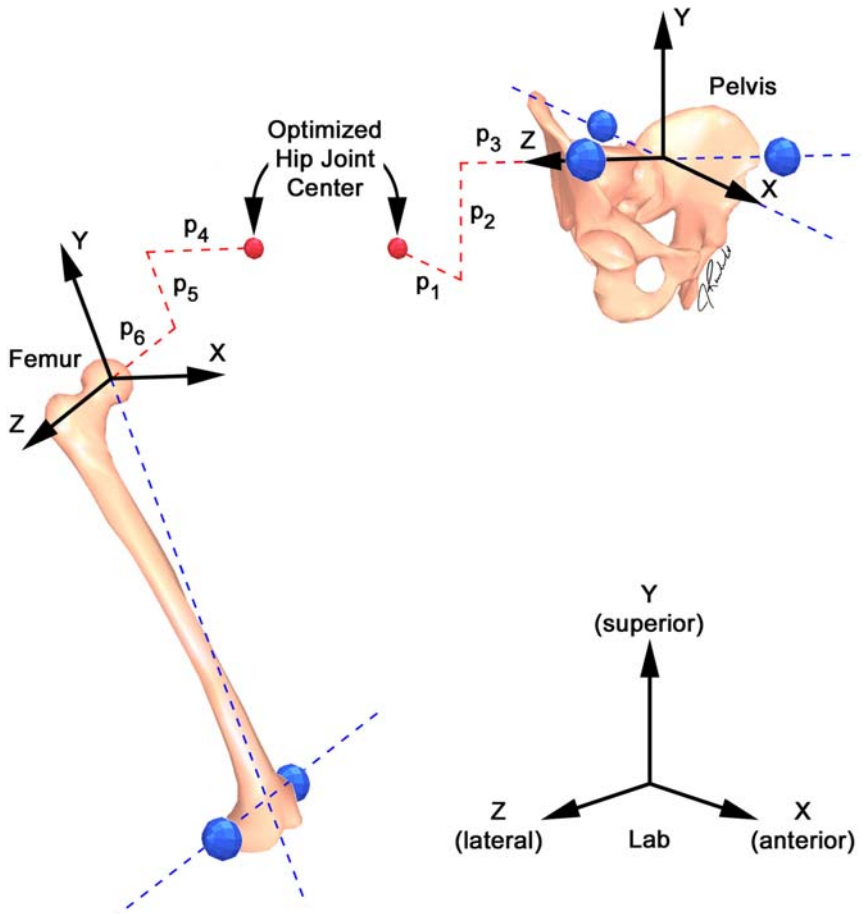

Figure 3-4. The 3 DOF right hip joint center simultaneously defined in the pelvis and right femur segments and the 6 translational model parameters optimized to determine the functional hip joint center location.

Table 3-2. Hip joint parameters.

Hip Joint Parameter	Description
p_1	Anterior-posterior location in pelvis segment
p_2	Superior-inferior location in pelvis segment
p_3	Medial-lateral location in pelvis segment
p_4	Anterior-posterior location in femur segment
p_5	Superior-inferior location in femur segment
p_6	Medial-lateral location in femur segment

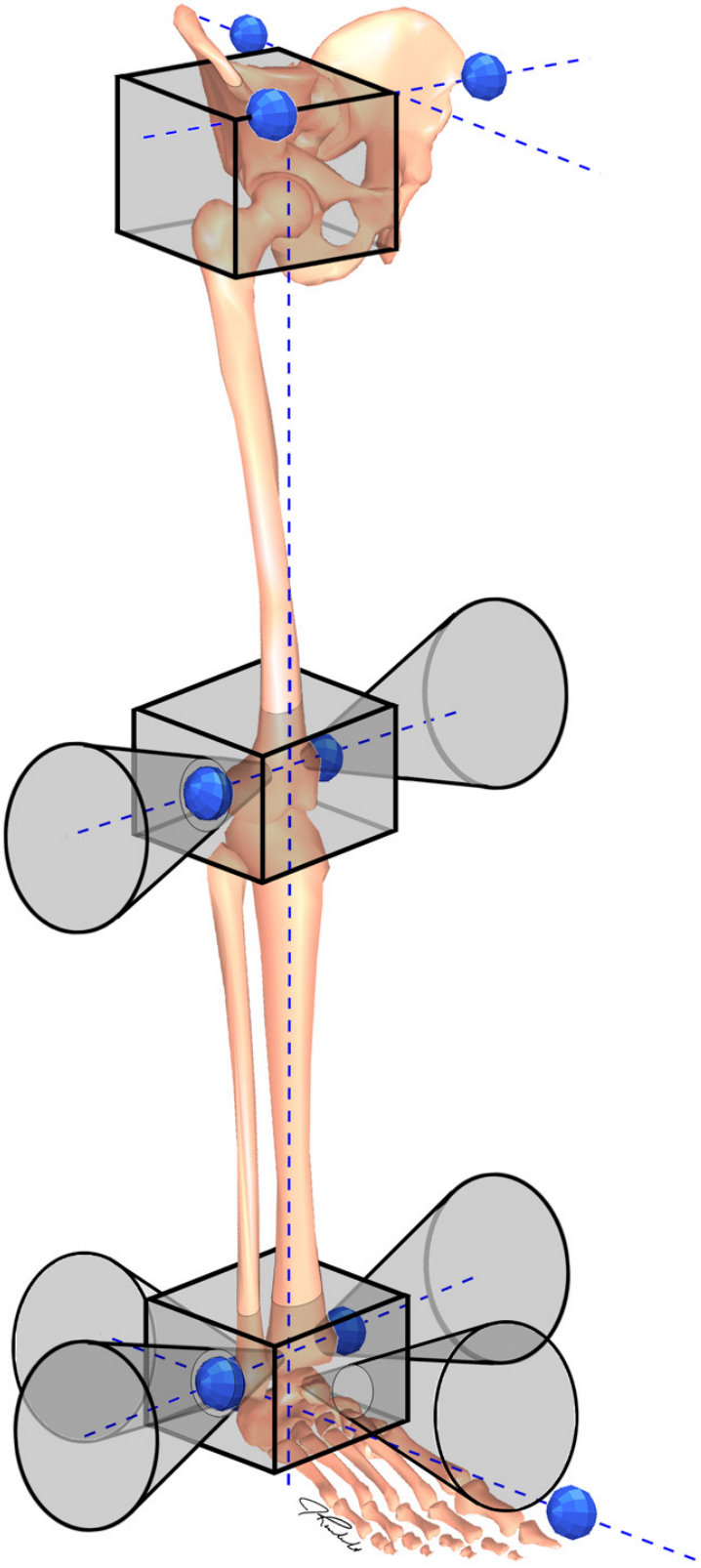

Figure 3-5. Geometric constraints on the optimization of translational and rotational model parameters for the hip, knee, and ankle joints.

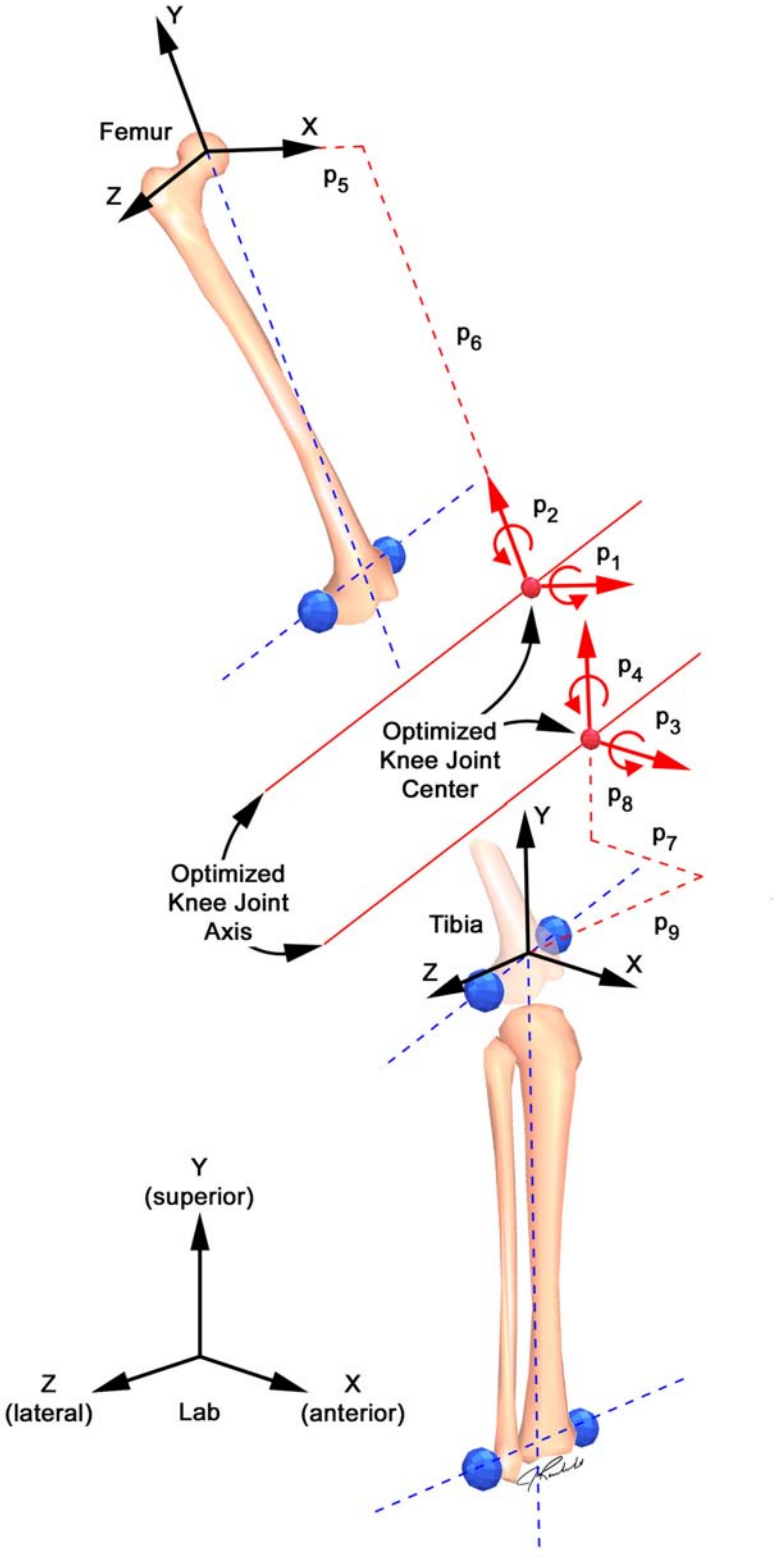

Figure 3-6. The 1 DOF right knee joint simultaneously defined in the right femur and right tibia segments and the 4 rotational and 5 translational model parameters optimized to determine the knee joint location and orientation.

Table 3-3. Knee joint parameters.

Knee Joint Parameter	Description
p_1	Adduction-abduction rotation in femur segment
p_2	Internal-external rotation in femur segment
p_3	Adduction-abduction rotation in tibia segment
p_4	Internal-external rotation in tibia segment
p_5	Anterior-posterior location in femur segment
p_6	Superior-inferior location in femur segment
p_7	Anterior-posterior location in tibia segment
p_8	Superior-inferior location in tibia segment
p_9	Medial-lateral location in tibia segment

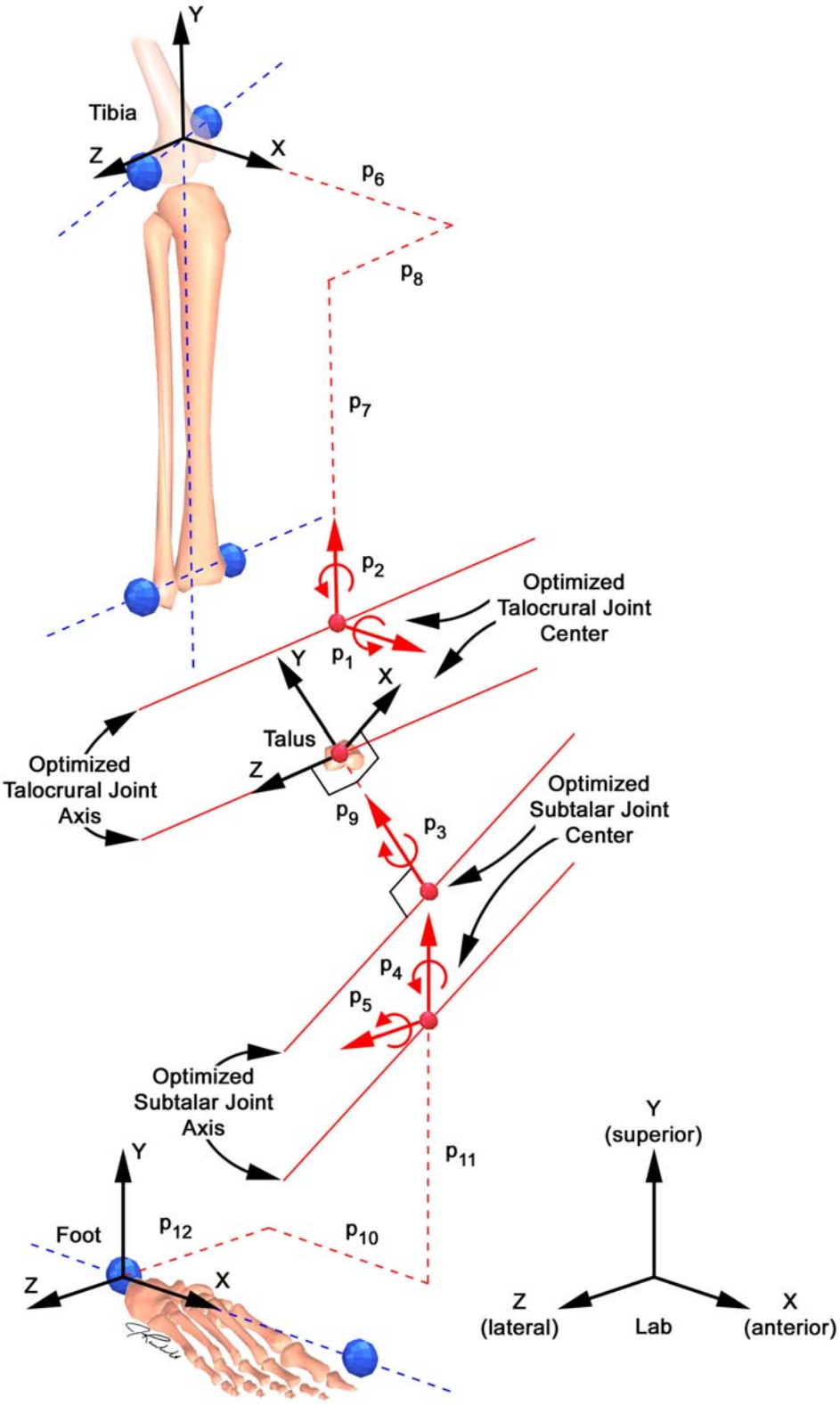

Figure 3-7. The 2 DOF right ankle joint complex simultaneously defined in the right tibia, talus, and foot segments and the 5 rotational and 7 translational model parameters optimized to determine the joint locations and orientations.

Table 3-4. Ankle joint parameters.

Ankle Joint Parameter	Description
p_1	Adduction-abduction rotation of talocrural in tibia segment
p_2	Internal-external rotation of talocrural in tibia segment
p_3	Internal-external rotation of subtalar in talus segment
p_4	Internal-external rotation of subtalar in foot segment
p_5	Dorsi-plantar rotation of subtalar in foot segment
p_6	Anterior-posterior location of talocrural in tibia segment
p_7	Superior-inferior location of talocrural in tibia segment
p_8	Medial-lateral location of talocrural in tibia segment
p_9	Superior-inferior location of subtalar in talus segment
p_{10}	Anterior-posterior location of subtalar in foot segment
p_{11}	Superior-inferior location of subtalar in foot segment
p_{12}	Medial-lateral location of subtalar in foot segment

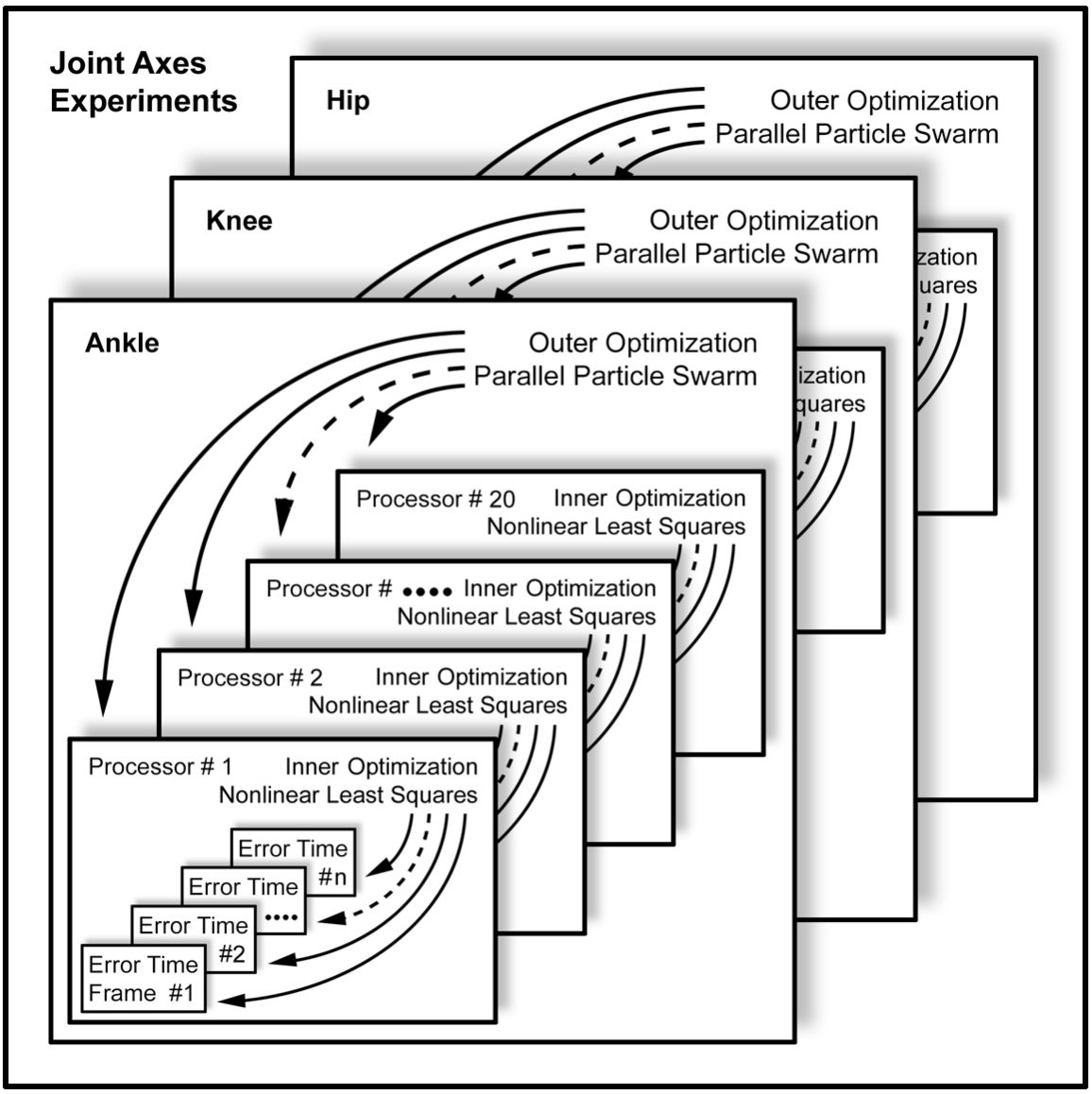

Figure 3-8. Two-level optimization technique minimizing the 3D marker coordinate errors between the kinematic model markers and experimental marker data to determine functional joint axes for each lower-extremity joint.

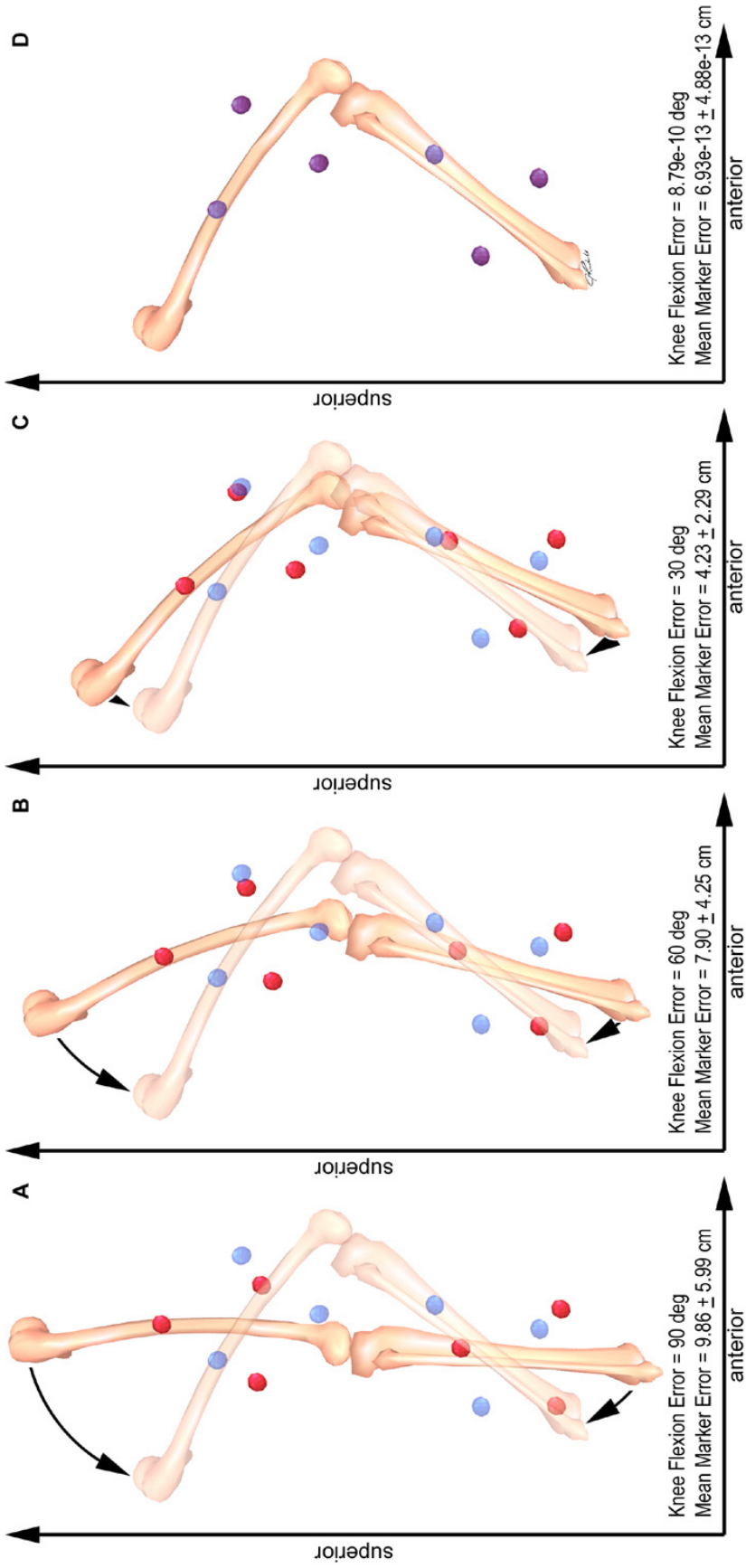

Figure 3-9. Inner-level optimization convergence illustration series for the knee joint, where synthetic markers are blue and model markers are red. Given synthetic marker data without noise, optimized outer-level design variables, and a synthetic knee flexion angle = 90°, A) is the initial model knee flexion = 0°, B) is the model knee flexion = 30°, C) is the model knee flexion = 60°, and D) is the final model knee flexion = 90°.

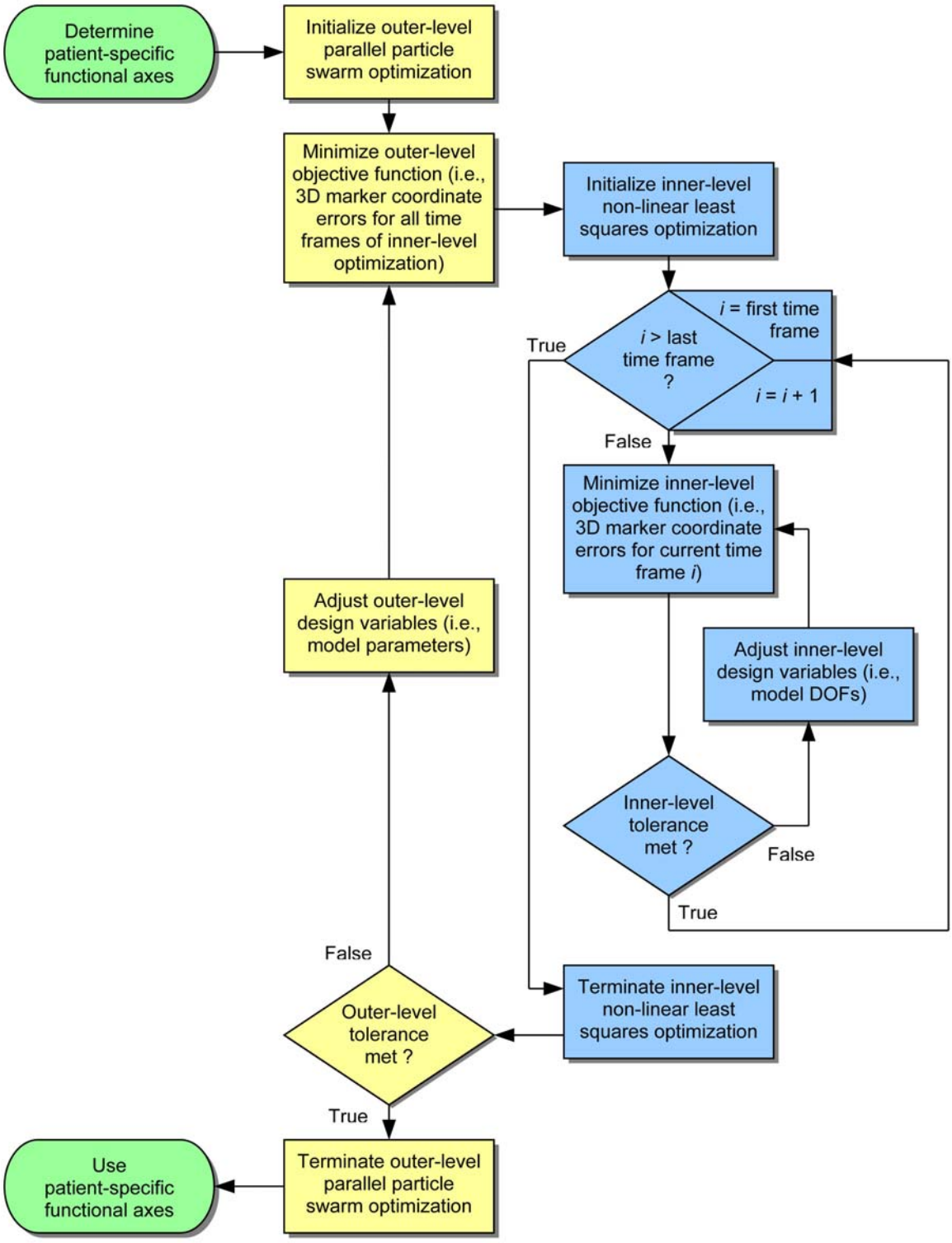

Figure 3-10. Two-level optimization approach minimizing the 3D marker coordinate errors between the kinematic model markers and experimental marker data to determine functional joint axes.

CHAPTER 4
RESULTS

Synthetic Marker Data without Noise

For synthetic motions without noise, each two-level optimization precisely recovered the original marker trajectories to within an arbitrarily tight tolerance (on the order of 1e-13 cm), as illustrated in Figure 3-9. At the termination of each optimization, the optimum model parameters for the hip, knee, and ankle were recovered with mean rotational errors less than or equal to 0.045° and mean translational errors less than or equal to 0.0077 cm (Appendix C).

Synthetic Marker Data with Noise

For synthetic motions with noise, the two-level optimization of the hip, knee, and ankle resulted in mean marker distance errors equal to 0.46 cm, which is of the same order of magnitude as the selected random continuous noise model (Table 4-1). The two-level approach determined the original model parameters with mean rotational errors less than or equal to 3.73° and mean translational errors less than or equal to 0.92 cm (Appendix D). The outer-level fitness history converged rapidly (Figure 4-1) and the hip, knee, and ankle optimizations terminated with a mean wall clock time of 41.02 hours.

Experimental Marker Data

For multi-cycle experimental motions, the mean marker distance error of the optimal hip, knee, and ankle solutions was 0.41 cm, which is a 0.43 cm improvement over the mean nominal error of 0.84 cm (Table 4-2). For each joint complex, the optimum model parameters improved upon the nominal parameter data (or values found

in the literature) by mean rotational values less than or equal to 6.18° and mean translational values less than or equal to 1.05 cm (Appendix E). When compared to the synthetic data with noise, the outer-level fitness history of the multi-cycle experimental data optimization converged at approximately the same rate and resulted in an improved final solution for both the ankle and the hip (Figure 4-2). On the contrary, the higher objective function values for the knee are evidence of the inability of the fixed pin joint to represent the screw-home motion (Blankevoort et al., 1988) of the multi-cycle experimental knee data. The multi-cycle hip, knee, and ankle optimizations terminated with a mean wall clock time of 35.94 hours.

For one-half-cycle experimental motions, the mean marker distance error of the optimal hip, knee, and ankle solutions was 0.30 cm for the first half and 0.30 cm for the second half (Table 4-3). The fitness of both the ankle and the hip were comparable to the multi-cycle joint motion results. However, the knee fitness values were improved due to the reduced influence (i.e., 1 time frame of data as opposed to 9) of the screw-home motion of the knee. For each joint complex, the optimum model parameters improved upon the nominal parameter data (or values found in the literature) by mean rotational values less than or equal to 11.08° and mean translational values less than or equal to 2.78 cm (Appendix F, Appendix G). In addition, the optimum model parameters for one-half-cycle motion differed from those for the multi-cycle motion by mean rotational values less than or equal to 15.77° and mean translational values less than or equal to 2.95 cm (Appendix H, Appendix I). The one-half-cycle hip, knee, and ankle optimizations terminated with a mean wall clock time of 11.77 hours.

Table 4-1. Two-level optimization results for synthetic marker data with random continuous numerical noise to simulate skin movement artifacts with maximum amplitude of 1 cm.

Synthetic Data with Noise	Hip	Knee	Ankle
Mean marker distance error (cm)	0.474603 ± 0.202248	0.392331 ± 0.145929	0.514485 ± 0.233956
Mean rotational parameter error (°)	n/a	2.158878 ± 1.288703	3.732191 ± 3.394553
Mean translational parameter error (cm)	0.161318 ± 0.039449	0.321930 ± 0.127997	0.923724 ± 0.471443

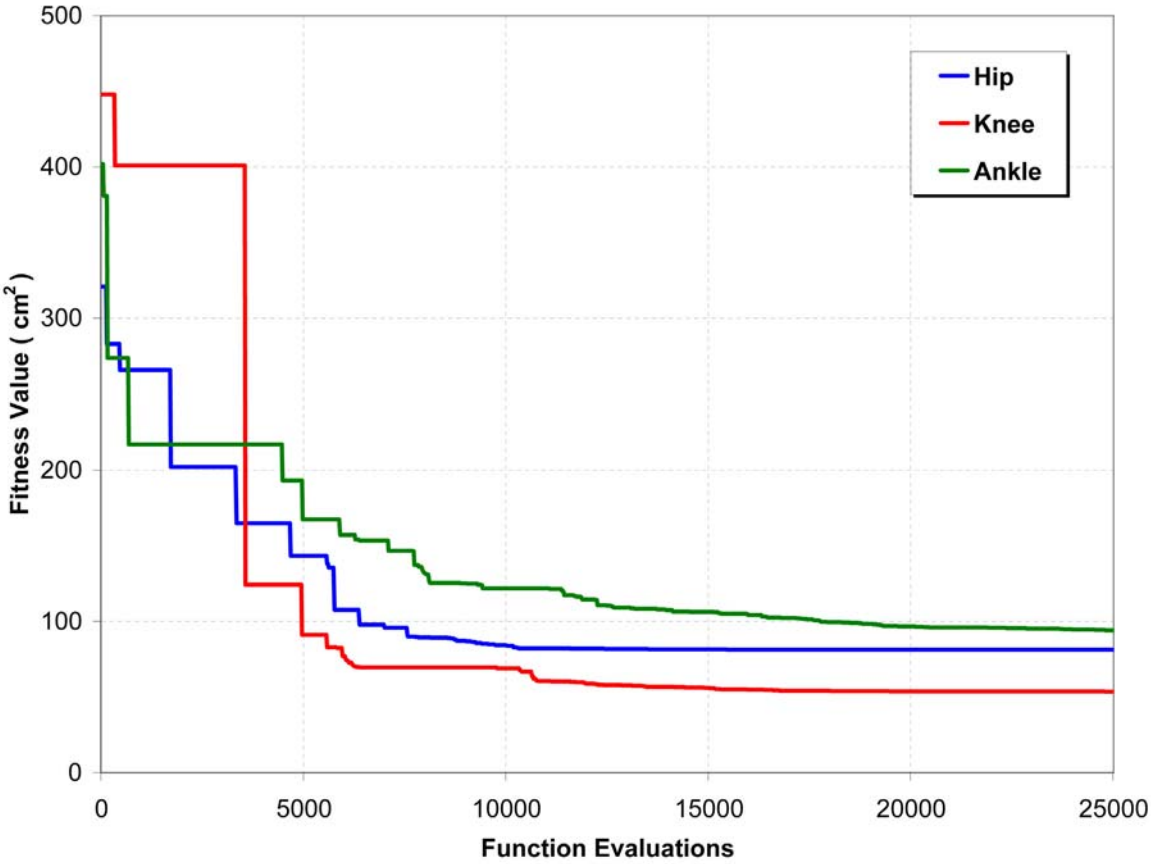

Figure 4-1. Outer-level optimization objective function fitness value convergence for synthetic marker data with random continuous numerical noise to simulate skin movement artifacts with maximum amplitude of 1 cm, where the best fitness value among all nodes is given for each iteration.

Table 4-2. Mean marker distance errors for nominal values and the two-level optimization results for multi-cycle experimental marker data.

Experimental Data	Hip	Knee	Ankle
Nominal mean marker distance error (cm)	0.499889 $\pm$ 0.177947	1.139884 $\pm$ 0.618567	0.885437 $\pm$ 0.478530
Optimum mean marker distance error (cm)	0.342262 $\pm$ 0.167079	0.547787 $\pm$ 0.269726	0.356279 $\pm$ 0.126559
Mean marker distance error attenuation (cm)	0.157627 $\pm$ 0.166236	0.592097 $\pm$ 0.443680	0.529158 $\pm$ 0.438157

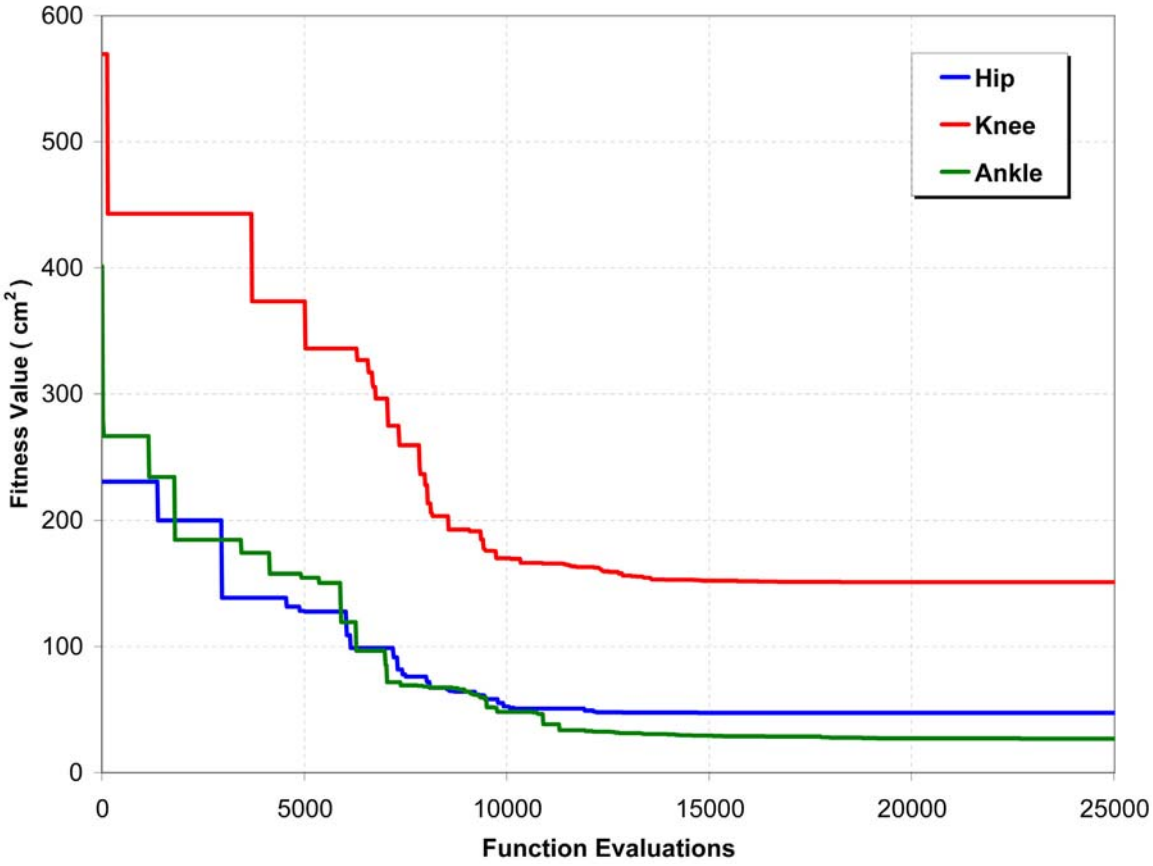

Figure 4-2. Outer-level optimization objective function fitness value convergence for multi-cycle experimental marker data, where the best fitness value among all nodes is given for each iteration.

Table 4-3. Mean marker distance errors for the two-level optimization results using first and second halves of the joint cycle motion for experimental marker data.

Experimental Data	Hip	Knee	Ankle
First half: mean marker distance error (cm)	0.335644 $\pm$ 0.163370	0.189551 $\pm$ 0.072996	0.384786 $\pm$ 0.193149
Second half: mean marker distance error (cm)	0.361179 $\pm$ 0.200774	0.202413 $\pm$ 0.101063	0.338886 $\pm$ 0.128596

CHAPTER 5
DISCUSSION

Assumptions, Limitations, and Future Work

Joint Model Selection

If the current model cannot adequately reproduce future experimental motions, the chosen joint models may be modified. For example, the flexion-extension of the knee is not truly represented by a fixed pin joint (Churchill et al., 1998). When comparing the fitness of the optimum knee joint model to multi-cycle experimental marker data, the agreement was quite good for all knee flexion angles with the exception of those approaching full extension. By eliminating knee flexion angles less than 20°, which comprised 18% of the flexion-extension data, the mean marker distance error was reduced to 0.48 ± 0.23 cm (11.89% decrease) using the optimum model parameters from the full data set. A pin joint knee may be sufficiently accurate for many modeling applications. A 2 DOF knee model (Hollister et al., 1993) may account for the screw-home motion of the knee joint occurring between 0° and 20° (Blankevoort et al., 1988). If greater fidelity to actual bone motion is necessary, a 6 DOF knee joint may be implemented with kinematics determined from fluoroscopy (Rahman et al., 2003).

Design Variable Constraints

Certain joint parameters must be constrained to zero with the purpose of preventing the unnecessary optimization of redundant parameters. Case in point, the medial-lateral translational model parameter placing the knee joint center in the femur segment must be constrained to zero. On the other hand, this model parameter may be used as a design

variable, granted the medial-lateral translational model parameter placing the knee joint center in the tibia segment is constrained to zero. If both medial-lateral translational model parameters are used as redundant design variables, the outer-level optimization has an infinite number of solutions within the constraints of both parameters. Through the elimination (i.e., constraining to zero) of redundant model parameters, the outer-level optimization encounters less convergence problems in globally minimizing the objective function.

Objective Function Formulation

The inner-level optimization objective function should be comprised of marker coordinate errors rather than marker distance errors. A substantial amount of information (i.e., ⅔ of the number of errors) describing the fitness value is lost with computation of marker distance errors. In other words, a marker distance error provides only the radius of a sphere surrounding an experimental marker and it does not afford the location of a model marker on the surface of the sphere. However, a set of three marker coordinate errors describes both the magnitude and direction of an error vector between an experimental marker and a model marker. By using marker coordinate errors, the inner-level optimization has improved convergence (Table 5-1) and shorter execution time (Table 5-2).

Optimization Time and Parallel Computing

To reduce the computation time, it is necessary to use an outer-level optimization algorithm in a parallel environment on a network cluster of processors. The PSO algorithm was chosen over gradient-based optimizers for its suitability to be parallelized and its ability to solve global optimization problems. The large computation time is a result of the random set of initial values used to seed each node of the parallel algorithm.

By seeding one of the nodes with a relatively optimal set of initial values, the computation time may be significantly decreased. By doubling the number of parallel processors, the computation time declines nearly 50%. Decreasing the number of time frames of marker data additionally reduces the computation time. For example, the mean optimization time using experimental data for 50 time frames equals 35.94 hours, 19 time frames equals 12.82 hours, and 13 time frames equals 11.24 hours. Further study is necessary to establish the minimum number of marker data time frames required to effectively determine joint axes parameters.

Multi-Cycle and One-Half-Cycle Joint Motions

The two-level optimization results vary depending on whether marker data time frames consist of multi-cycle or one-half-cycle joint motions. In other words, the determination of patient-specific model parameters is significantly influenced by the marker trajectories contained within the chosen set of data. Given a set of marker data, the two-level optimization establishes invariable model parameters that best fit the mathematical model to the measured experimental motion. Understandably, a model constructed from one marker data set may not adequately represent a considerably different marker data set. To perform accurate dynamic analyses, joint motions used to generate the model should be consistent with those motions that will be used in the analyses.

The small differences between sets of two-level optimization results for the hip and knee joint motions indicate the reliability of the model parameter values. Much larger differences occurred between sets of model parameters determined for the ankle joint. Two major factors contributing to these differences are the rotational ankle model parameters p_1 and p_3. On one hand, the model parameters may truly vary throughout the

ankle motion and may not be represented by constant values. On the other hand, the objective function may be insensitive to changes in these model parameters indicating a design space that does not permit the reasonable determination of certain design variables. Future study is necessary to investigate the sensitivity of 3D marker coordinate errors to particular model parameters.

Range of Motion and Loading Conditions

To provide the largest range of motion, all experimental data was collected with each joint unloaded and freely exercising all DOFs; however, the same two-level optimization may be performed on loaded data as well. The patient-specific model parameters may change under loaded conditions (Bogert et al., 1994). Moreover, loaded conditions limit the range of motion for several DOFs. Several authors (Bell et al., 1990; Bogert et al., 1994) report inaccuracies in determining functional axes from limited motion, but a subsequent study (Piazza et al., 2001) found the hip joint may be determined from motions as small as 15°. Piazza et al. (2001) suggest future studies are necessary to explore the use of normal gait motions, rather than special joint motions, to determine functional axes.

Optimization Using Gait Motion

The two-level optimization approach and synthetic data evaluation method may be used to investigate the use of gait motion to determine functional joint axes. Each set of joint parameters may be established separately or collectively (i.e., entire single leg or both legs at once). Additional investigation is necessary to assess the differences in joint parameters obtained through individual optimizations and simultaneous whole leg optimizations. Furthermore, the joint parameters determined from gait motions may be

compared to those parameters obtained from special joint motions with larger amounts of movement.

Authors (Bogert et al., 1994; Chéze et al., 1995; Lu and O'Connor, 1999) have set precedence for performing numerical (or synthetic data) simulations to evaluate a new technique. Although it is not a necessary task, there is additional benefit in supporting the numerical findings with data from one human subject. With the additional data, the joint parameters computed from unloaded joint motions may be measured against those parameters attained from unloaded (i.e., swing phase) and loaded (i.e., stance phase) gait motions. To expand upon the evaluation of the new technique and show general applicability, future work is necessary to study more than one human subject.

Comparison of Experimental Results with Literature

The two-level optimization determined patient-specific joint axes locations and orientations similar to previous works. The optimum hip joint center location of 7.52 cm (27.89% posterior), 9.27 cm (34.38% inferior), and 8.86 cm (32.85% lateral) are respectively comparable to 19.3%, 30.4%, and 35.9% (Bell et al., 1990). The optimum femur length (40.46 cm) and tibia length (40.88 cm) are similar to 42.22 cm and 43.40 cm, respectively (de Leva, 1996). The optimum coronal plane rotation (73.36°) of the talocrural joint correlates to 82.7 $\pm$ 3.7° (range 74° to 94°) (Inman, 1976). The optimum distance (2.14 cm) between the talocrural joint and the subtalar joint is analogous to 1.24 $\pm$ 0.29 cm (Bogert et al., 1994). The optimum transverse plane rotation (13.19°) and sagittal plane rotation (45.26°) of the subtalar joint corresponds to 23 $\pm$ 11° (range 4° to 47°) and 42 $\pm$ 9° (range 20.5° to 68.5°), respectively (Inman, 1976).

Table 5-1. Mean marker distance errors for the inner-level objective function consisting of marker coordinate errors versus marker distance errors for multi-cycle experimental marker data.

Experimental Data	Hip	Knee	Ankle
Marker distance objective function: mean marker distance error (cm)	0.863941 ± 0.328794	1.043909 ± 0.465186	0.674187 ± 0.278451
Marker coordinate objective function: mean marker distance error (cm)	0.342262 ± 0.167079	0.547787 ± 0.269726	0.356279 ± 0.126559

Table 5-2. Execution times for the inner-level objective function consisting of marker coordinate errors versus marker distance errors for multi-cycle experimental marker data.

Experimental Data	Hip	Knee	Ankle
Marker distance objective function: execution time (s)	464.377	406.205	308.293
Marker coordinate objective function: execution time (s)	120.414	106.003	98.992

CHAPTER 6
CONCLUSION

Rationale for New Approach

The main motivation for developing a 27 DOF patient-specific computational model and a two-level optimization method to enhance the lower-extremity portion is to predict the post-surgery peak knee adduction moment in HTO patients, which has been identified as an indicator of clinical outcome (Andriacchi, 1994; Bryan et al., 1997; Hurwitz et al., 1998; Prodromos et al., 1985; Wang et al., 1990). The accuracy of prospective dynamic analyses made for a unique patient is determined in part by the fitness of the underlying kinematic model (Andriacchi and Strickland, 1985; Challis and Kerwin, 1996; Cappozzo et al., 1975; Davis, 1992; Holden and Stanhope, 1998; Holden and Stanhope, 2000; Stagni et al., 2000). Development of an accurate kinematic model tailored to a specific patient forms the groundwork toward creating a predictive patient-specific dynamic simulation.

Synthesis of Current Work and Literature

The two-level optimization method satisfactorily determines patient-specific model parameters defining a 3D lower-extremity model that is well suited to a particular patient. Two conclusions may be drawn from comparing and contrasting the two-level optimization results to previous values found in the literature. The similarities between numbers suggest the results are reasonable and show the extent of agreement with past studies. The differences between values indicate the two-level optimization is necessary

and demonstrate the degree of inaccuracy inherent when the new approach is not implemented.

Through the enhancement of model parameter values found in the literature, the two-level optimization approach successfully reduces the fitness errors between the patient-specific model and the experimental motion data. More specifically, to quantify the improvement of the current results compared to previous values found in the literature, the mean marker distance errors were reduced by 31.53% (hip), 51.94% (knee), and 59.76% (ankle).

The precision of dynamic analyses made for a particular patient depends on the accuracy of the patient-specific kinematic parameters chosen for the dynamic model. Without expensive medical images, model parameters are only estimated from external landmarks that have been identified in previous studies. The estimated (or nominal) values may be improved by formulating an optimization problem using motion-capture data. By using a two-level optimization technique, researchers may build more accurate biomechanical models of the individual human structure. As a result, the optimal models will provide reliable foundations for future dynamic analyses and optimizations.

GLOSSARY

Abduction	Movement away from the midline of the body in the coronal plane.
Acceleration	The time rate of change of velocity.
Active markers	Joint and segment markers used during motion capture that emit a signal.
Adduction	Movement towards the midline of the body in the coronal plane.
Ankle inversion-eversion	Motion of the long axis of the foot within the coronal plane as seen by an observer positioned along the anterior-posterior axis of the shank.
Ankle motion	The ankle angles reflect the motion of the foot segment relative to the shank segment.
Ankle plantarflexion-dorsiflexion	Motion of the plantar aspect of the foot within the sagittal plane as seen by an observer positioned along the medial-lateral axis of the shank.
Anterior	The front or before, also referred to as ventral.
Circumduction	Movement of the distal tip of a segment described by a circle.
Coccyx	The tailbone located at the distal end of the sacrum.
Constraint functions	Specific limits that must be satisfied by the optimal design.
Coronal plane	The plane that divides the body or body segment into anterior and posterior parts.
Couple	A set of force vectors whose resultant is equal to zero. Two force vectors with equal magnitudes and opposite directions is an example of a simple couple.

Degree of freedom (DOF)	A single coordinate of relative motion between two bodies. Such a coordinate responds without constraint or imposed motion to externally applied forces or torques. For translational motion, a DOF is a linear coordinate along a single direction. For rotational motion, a DOF is an angular coordinate about a single, fixed axis.
Design variables	Variables that change to optimize the design.
Distal	Away from the point of attachment or origin.
Dorsiflexion	Movement of the foot towards the anterior part of the tibia in the sagittal plane.
Epicondyle	Process that develops proximal to an articulation and provides additional surface area for muscle attachment.
Eversion	A turning outward.
Extension	Movement that rotates the bones comprising a joint away from each other in the sagittal plane.
External (lateral) rotation	Movement that rotates the distal segment laterally in relation to the proximal segment in the transverse plane, or places the anterior surface of a segment away from the longitudinal axis of the body.
External moment	The load applied to the human body due to the ground reaction forces, gravity and external forces.
Femur	The longest and heaviest bone in the body. It is located between the hip joint and the knee joint.
Flexion	Movement that rotates the bones comprising a joint towards each other in the sagittal plane.
Fluoroscopy	Examination of body structures using an X-ray machine that combines an X-ray source and a fluorescent screen to enable real-time observation.
Force	A push or a pull and is produced when one object acts on another.

Force plate	A transducer that is set in the floor to measure about some specified point, the force and torque applied by the foot to the ground. These devices provide measures of the three components of the resultant ground reaction force vector and the three components of the resultant torque vector.
Forward dynamics	Analysis to determine the motion of a mechanical system, given the topology of how bodies are connected, the applied forces and torques, the mass properties, and the initial condition of all degrees of freedom.
Gait	A manner of walking or moving on foot.
Generalized coordinates	A set of coordinates (or parameters) that uniquely describes the geometric position and orientation of a body or system of bodies. Any set of coordinates that are used to describe the motion of a physical system.
High tibial osteotomy (HTO)	Surgical procedure that involves adding or removing a wedge of bone to or from the tibia and changing the frontal plane limb alignment. The realignment shifts the weight-bearing axis from the diseased medial compartment to the healthy lateral compartment of the knee.
Hip abduction-adduction	Motion of a long axis of the thigh within the coronal plane as seen by an observer positioned along the anterior-posterior axis of the pelvis.
Hip flexion-extension	Motion of the long axis of the thigh within the sagittal plane as seen by an observer positioned along the medial-lateral axis of the pelvis.
Hip internal-external rotation	Motion of the medial-lateral axis of the thigh with respect to the medial-lateral axis of the pelvis within the transverse plane as seen by an observer positioned along the longitudinal axis of the thigh.
Hip motion	The hip angles reflect the motion of the thigh segment relative to the pelvis.
Inferior	Below or at a lower level (towards the feet).

Inter-ASIS distance	The length of measure between the left anterior superior iliac spine (ASIS) and the right ASIS.
Internal (medial) rotation	Movement that rotates the distal segment medially in relation to the proximal segment in the transverse plane, or places the anterior surface of a segment towards the longitudinal axis of the body.
Internal joint moments	The net result of all the internal forces acting about the joint which include moments due to muscles, ligaments, joint friction and structural constraints. The joint moment is usually calculated around a joint center.
Inverse dynamics	Analysis to determine the forces and torques necessary to produce the motion of a mechanical system, given the topology of how bodies are connected, the kinematics, the mass properties, and the initial condition of all degrees of freedom.
Inversion	A turning inward.
Kinematics	Those parameters that are used in the description of movement without consideration for the cause of movement abnormalities. These typically include parameters such as linear and angular displacements, velocities and accelerations.
Kinetics	General term given to the forces that cause movement. Both internal (muscle activity, ligaments or friction in muscles and joints) and external (ground or external loads) forces are included. The moment of force produced by muscles crossing a joint, the mechanical power flowing to and from those same muscles, and the energy changes of the body that result from this power flow are the most common kinetic parameters used.
Knee abduction-adduction	Motion of the long axis of the shank within the coronal plane as seen by an observer positioned along the anterior-posterior axis of the thigh.
Knee flexion-extension	Motion of the long axis of the shank within the sagittal plane as seen by an observer positioned along the medial-lateral axis of the thigh.

Knee internal-external rotation	Motion of the medial-lateral axis of the shank with respect to the medial-lateral axis of the thigh within the transverse plane as viewed by an observer positioned along the longitudinal axis of the shank.
Knee motion	The knee angles reflect the motion of the shank segment relative to the thigh segment.
Lateral	Away from the body's longitudinal axis, or away from the midsagittal plane.
Malleolus	Broadened distal portion of the tibia and fibula providing lateral stability to the ankle.
Markers	Active or passive objects (balls, hemispheres or disks) aligned with respect to specific bony landmarks used to help determine segment and joint position in motion capture.
Medial	Toward the body's longitudinal axis, or toward the midsagittal plane.
Midsagittal plane	The plane that passes through the midline and divides the body or body segment into the right and left halves.
Model parameters	A set of coordinates that uniquely describes the model segments lengths, joint locations, and joint orientations, also referred to as joint parameters. Any set of coordinates that are used to describe the geometry of a model system.
Moment of force	The moment of force is calculated about a point and is the cross product of a position vector from the point to the line of action for the force and the force. In two-dimensions, the moment of force about a point is the product of a force and the perpendicular distance from the line of action of the force to the point. Typically, moments of force are calculated about the center of rotation of a joint.
Motion capture	Interpretation of computerized data that documents an individual's motion.

Non-equidistant	The opposite of equal amounts of distance between two or more points, or not equally distanced.
Objective functions	Figures of merit to be minimized or maximized.
Parametric	Of or relating to or in terms of parameters, or factors that define a system.
Passive markers	Joint and segment markers used during motion capture that reflect visible or infrared light.
Pelvis	Consists of the two hip bones, the sacrum, and the coccyx. It is located between the proximal spine and the hip joints.
Pelvis anterior-posterior tilt	Motion of the long axis of the pelvis within the sagittal plane as seen by an observer positioned along the medial-lateral axis of the laboratory.
Pelvis elevation-depression	Motion of the medial-lateral axis of the pelvis within the coronal plane as seen by an observer positioned along the anterior-posterior axis of the laboratory.
Pelvis internal-external rotation	Motion of the medial-lateral or anterior-posterior axis of the pelvis within the transverse plane as seen by an observer positioned along the longitudinal axis of the laboratory.
Pelvis motion	The position of the pelvis as defined by a marker set (for example, plane formed by the markers on the right and left anterior superior iliac spine (ASIS) and a marker between the 5^{th} lumbar vertebrae and the sacrum) relative to a laboratory coordinate system.
Plantarflexion	Movement of the foot away from the anterior part of the tibia in the sagittal plane.
Posterior	The back or behind, also referred to as dorsal.
Proximal	Toward the point of attachment or origin.
Range of motion	Indicates joint motion excursion from the maximum angle to the minimum angle.

Sacrum	Consists of the fused components of five sacral vertebrae located between the 5th lumbar vertebra and the coccyx. It attaches the axial skeleton to the pelvic girdle of the appendicular skeleton via paired articulations.
Sagittal plane	The plane that divides the body or body segment into the right and left parts.
Skin movement artifacts	The relative movement between skin and underlying bone.
Stance phase	The period of time when the foot is in contact with the ground.
Subtalar joint	Located between the distal talus and proximal calcaneous, also known as the talocalcaneal joint.
Superior	Above or at a higher level (towards the head).
Synthetic markers	Computational representations of passive markers located on the kinematic model.
Swing phase	The period of time when the foot is not in contact with the ground.
Talocrural joint	Located between the distal tibia and proximal talus, also known as the tibial-talar joint.
Talus	The largest bone of the ankle transmitting weight from the tibia to the rest of the foot.
Tibia	The large medial bone of the lower leg, also known as the shinbone. It is located between the knee joint and the talocrural joint.
Transepicondylar	The line between the medial and lateral epicondyles.
Transverse plane	The plane at right angles to the coronal and sagittal planes that divides the body into superior and inferior parts.
Velocity	The time rate of change of displacement.

APPENDIX A
NOMINAL JOINT PARAMETERS & OPTIMIZATION BOUNDS FOR SYNTHETIC MARKER DATA

Table A-1. Nominal right hip joint parameters and optimization bounds for synthetic marker data.

Right Hip Joint Parameter	Nominal	Lower Bound	Upper Bound
p_1 (cm)	-6.022205	-20.530245	0
p_2 (cm)	-9.307044	-20.530245	0
p_3 (cm)	8.759571	0	20.530245
p_4 (cm)	0	-14.508040	6.022205
p_5 (cm)	0	-11.223200	9.307044
p_6 (cm)	0	-8.759571	11.770674

Table A-2. Nominal right knee joint parameters and optimization bounds for synthetic marker data.

Right Knee Joint Parameter	Nominal	Lower Bound	Upper Bound
p_1 (°)	0	-30	30
p_2 (°)	0	-30	30
p_3 (°)	-5.079507	-35.079507	24.920493
p_4 (°)	16.301928	-13.698072	46.301928
p_5 (cm)	0	-7.836299	7.836299
p_6 (cm)	-37.600828	-45.437127	-29.764528
p_7 (cm)	0	-7.836299	7.836299
p_8 (cm)	0	-7.836299	7.836299
p_9 (cm)	0	-7.836299	7.836299

Table A-3. Nominal right ankle joint parameters and optimization bounds for synthetic marker data.

Right Ankle Joint Parameter	Nominal	Lower Bound	Upper Bound
p_1 (°)	18.366935	-11.633065	48.366935
p_2 (°)	0	-30	30
p_3 (°)	40.230969	10.230969	70.230969
p_4 (°)	23	-7	53
p_5 (°)	42	12	72
p_6 (cm)	0	-6.270881	6.270881
p_7 (cm)	-39.973202	-46.244082	-33.702321
p_8 (cm)	0	-6.270881	6.270881
p_9 (cm)	-1	-6.270881	0
p_{10} (cm)	8.995334	2.724454	15.266215
p_{11} (cm)	4.147543	-2.123338	10.418424
p_{12} (cm)	0.617217	-5.653664	6.888097

APPENDIX B
NOMINAL JOINT PARAMETERS & OPTIMIZATION BOUNDS FOR EXPERIMENTAL MARKER DATA

Table B-1. Nominal right hip joint parameters and optimization bounds for experimental marker data.

Right Hip Joint Parameter	Nominal	Lower Bound	Upper Bound
p_1 (cm)	-5.931423	-20.220759	0
p_2 (cm)	-9.166744	-20.220759	0
p_3 (cm)	8.627524	0	20.220759
p_4 (cm)	0	-14.289337	5.931423
p_5 (cm)	0	-11.054015	9.166744
p_6 (cm)	0	-8.627524	11.593235

Table B-2. Nominal right knee joint parameters and optimization bounds for experimental marker data.

Right Knee Joint Parameter	Nominal	Lower Bound	Upper Bound
p_1 (°)	0	-30	30
p_2 (°)	0	-30	30
p_3 (°)	-4.070601	-34.070601	25.929399
p_4 (°)	1.541414	-28.458586	31.541414
p_5 (cm)	0	-7.356876	7.356876
p_6 (cm)	-39.211319	-46.568195	-31.854442
p_7 (cm)	0	-7.356876	7.356876
p_8 (cm)	0	-7.356876	7.356876
p_9 (cm)	0	-7.356876	7.356876

Table B-3. Nominal right ankle joint parameters and optimization bounds for experimental marker data.

Right Ankle Joint Parameter	Nominal	Lower Bound	Upper Bound
p_1 (°)	8.814964	-21.185036	38.814964
p_2 (°)	0	-30	30
p_3 (°)	26.890791	-3.109209	56.890791
p_4 (°)	23	-7	53
p_5 (°)	42	12	72
p_6 (cm)	0	-5.662309	5.662309
p_7 (cm)	-41.131554	-46.793862	-35.469245
p_8 (cm)	0	-5.662309	5.662309
p_9 (cm)	-1	-5.662309	0
p_{10} (cm)	9.113839	3.451530	14.776147
p_{11} (cm)	3.900829	-1.761479	9.563138
p_{12} (cm)	1.116905	-4.545403	6.779214

APPENDIX C
NOMINAL & OPTIMUM JOINT PARAMETERS FOR SYNTHETIC MARKER DATA WITHOUT NOISE

Table C-1. Nominal and optimum right hip joint parameters for synthetic marker data without noise.

Right Hip Joint Parameter	Nominal	Optimized	Error
p_1 (cm)	-6.022205	-6.022205	0.000000
p_2 (cm)	-9.307044	-9.307041	0.000003
p_3 (cm)	8.759571	8.759578	0.000007
p_4 (cm)	0	0.000004	0.000004
p_5 (cm)	0	0.000015	0.000015
p_6 (cm)	0	-0.000008	0.000008

Table C-2. Nominal and optimum right knee joint parameters for synthetic marker data without noise.

Right Knee Joint Parameter	Nominal	Optimized	Error
p_1 (°)	0	-0.040222	0.040222
p_2 (°)	0	-0.051509	0.051509
p_3 (°)	-5.079507	-5.050744	0.028763
p_4 (°)	16.301928	16.242914	0.059015
p_5 (cm)	0	-0.009360	0.009360
p_6 (cm)	-37.600828	-37.589068	0.011760
p_7 (cm)	0	-0.014814	0.014814
p_8 (cm)	0	-0.002142	0.002142
p_9 (cm)	0	-0.000189	0.000189

Table C-3. Nominal and optimum right ankle joint parameters for synthetic marker data without noise.

Right Ankle Joint Parameter	Nominal	Optimized	Error
p_1 (°)	18.366935	18.364964	0.001971
p_2 (°)	0	-0.011809	0.011809
p_3 (°)	40.230969	40.259663	0.028694
p_4 (°)	23	23.027088	0.027088
p_5 (°)	42	42.002080	0.002080
p_6 (cm)	0	0.000270	0.000270
p_7 (cm)	-39.973202	-39.972852	0.000350
p_8 (cm)	0	-0.000287	0.000287
p_9 (cm)	-1	-1.000741	0.000741
p_{10} (cm)	8.995334	8.995874	0.000540
p_{11} (cm)	4.147543	4.147353	0.000190
p_{12} (cm)	0.617217	0.616947	0.000270

APPENDIX D
NOMINAL & OPTIMUM JOINT PARAMETERS FOR SYNTHETIC MARKER DATA WITH NOISE

Table D-1. Nominal and optimum right hip joint parameters for synthetic marker data with noise.

Right Hip Joint Parameter	Nominal	Optimized	Error
p_1 (cm)	-6.022205	-5.854080	0.168125
p_2 (cm)	-9.307044	-9.434820	0.127776
p_3 (cm)	8.759571	8.967520	0.207949
p_4 (cm)	0	0.092480	0.092480
p_5 (cm)	0	-0.180530	0.180530
p_6 (cm)	0	0.191050	0.191050

Table D-2. Nominal and optimum right knee joint parameters for synthetic marker data with noise.

Right Knee Joint Parameter	Nominal	Optimized	Error
p_1 (°)	0	-3.295650	3.295650
p_2 (°)	0	-1.277120	1.277120
p_3 (°)	-5.079507	-5.604100	0.524593
p_4 (°)	16.301928	12.763780	3.538148
p_5 (cm)	0	0.375600	0.375600
p_6 (cm)	-37.600828	-37.996910	0.396082
p_7 (cm)	0	0.489510	0.489510
p_8 (cm)	0	0.144040	0.144040
p_9 (cm)	0	-0.204420	0.204420

Table D-3. Nominal and optimum right ankle joint parameters for synthetic marker data with noise.

Right Ankle Joint Parameter	Nominal	Optimized	Error
p_1 (°)	18.366935	15.130096	3.236838
p_2 (°)	0	8.007498	8.007498
p_3 (°)	40.230969	32.975096	7.255873
p_4 (°)	23	23.122015	0.122015
p_5 (°)	42	42.038733	0.038733
p_6 (cm)	0	-0.398360	0.398360
p_7 (cm)	-39.973202	-39.614220	0.358982
p_8 (cm)	0	-0.755127	0.755127
p_9 (cm)	-1	-2.816943	1.816943
p_{10} (cm)	8.995334	10.210540	1.215206
p_{11} (cm)	4.147543	3.033673	1.113870
p_{12} (cm)	0.617217	-0.190367	0.807584

APPENDIX E
NOMINAL & OPTIMUM JOINT PARAMETERS FOR MULTI-CYCLE EXPERIMENTAL MARKER DATA

Table E-1. Nominal and optimum right hip joint parameters for multi-cycle experimental marker data.

Right Hip Joint Parameter	Nominal	Optimized	Improvement
p_1 (cm)	-5.931423	-7.518819	1.587396
p_2 (cm)	-9.166744	-9.268741	0.101997
p_3 (cm)	8.627524	8.857706	0.230182
p_4 (cm)	0	-2.123433	2.123433
p_5 (cm)	0	0.814089	0.814089
p_6 (cm)	0	1.438188	1.438188

Table E-2. Nominal and optimum right knee joint parameters for multi-cycle experimental marker data.

Right Knee Joint Parameter	Nominal	Optimized	Improvement
p_1 (°)	0	-0.586205	0.586205
p_2 (°)	0	14.854951	14.854951
p_3 (°)	-4.070601	-2.724374	1.346227
p_4 (°)	1.541414	2.404475	0.863061
p_5 (cm)	0	-1.422101	1.422101
p_6 (cm)	-39.211319	-39.611720	0.400401
p_7 (cm)	0	-0.250043	0.250043
p_8 (cm)	0	-0.457104	0.457104
p_9 (cm)	0	1.471656	1.471656

Table E-3. Nominal and optimum right ankle joint parameters for multi-cycle experimental marker data.

Right Ankle Joint Parameter	Nominal	Optimized	Improvement
p_1 (°)	8.814964	16.640499	7.825535
p_2 (°)	0	9.543288	9.543288
p_3 (°)	26.890791	27.359342	0.468551
p_4 (°)	23	13.197304	9.802696
p_5 (°)	42	45.259512	3.259512
p_6 (cm)	0	1.650689	1.650689
p_7 (cm)	-41.131554	-41.185800	0.054246
p_8 (cm)	0	-1.510034	1.510034
p_9 (cm)	-1	-2.141939	1.141939
p_{10} (cm)	9.113839	11.244080	2.130241
p_{11} (cm)	3.900829	3.851262	0.049567
p_{12} (cm)	1.116905	0.283095	0.833810

APPENDIX F
NOMINAL & OPTIMUM JOINT PARAMETERS FOR FIRST ONE-HALF-CYCLE EXPERIMENTAL MARKER DATA

Table F-1. Nominal and optimum right hip joint parameters for first one-half-cycle experimental marker data.

Right Hip Joint Parameter	Nominal	Optimized	Improvement
p_1 (cm)	-5.931423	-7.377948	1.446525
p_2 (cm)	-9.166744	-9.257734	0.090990
p_3 (cm)	8.627524	8.124560	0.502964
p_4 (cm)	0	-2.050133	2.050133
p_5 (cm)	0	0.813034	0.813034
p_6 (cm)	0	0.656323	0.656323

Table F-2. Nominal and optimum right knee joint parameters for first one-half-cycle experimental marker data.

Right Knee Joint Parameter	Nominal	Optimized	Improvement
p_1 (°)	0	7.621903	7.621903
p_2 (°)	0	12.823259	12.823259
p_3 (°)	-4.070601	-0.642569	3.428032
p_4 (°)	1.541414	11.252668	9.711254
p_5 (cm)	0	-1.217316	1.217316
p_6 (cm)	-39.211319	-38.611100	0.600219
p_7 (cm)	0	-1.252732	1.252732
p_8 (cm)	0	-0.003903	0.003903
p_9 (cm)	0	1.480035	1.480035

Table F-3. Nominal and optimum right ankle joint parameters for first one-half-cycle experimental marker data.

Right Ankle Joint Parameter	Nominal	Optimized	Improvement
p_1 (°)	8.814964	-15.959751	24.774715
p_2 (°)	0	-4.522393	4.522393
p_3 (°)	26.890791	18.986137	7.904654
p_4 (°)	23	28.588479	5.588479
p_5 (°)	42	36.840527	5.159473
p_6 (cm)	0	3.624386	3.624386
p_7 (cm)	-41.131554	-43.537980	2.406426
p_8 (cm)	0	-3.370814	3.370814
p_9 (cm)	-1	-2.246233	1.246233
p_{10} (cm)	9.113839	12.155750	3.041911
p_{11} (cm)	3.900829	0.488739	3.412090
p_{12} (cm)	1.116905	-1.207070	2.323975

APPENDIX G
NOMINAL & OPTIMUM JOINT PARAMETERS FOR SECOND ONE-HALF-CYCLE EXPERIMENTAL MARKER DATA

Table G-1. Nominal and optimum right hip joint parameters for second one-half-cycle experimental marker data.

Right Hip Joint Parameter	Nominal	Optimized	Improvement
p_1 (cm)	-5.931423	-7.884120	1.952697
p_2 (cm)	-9.166744	-10.160573	0.993829
p_3 (cm)	8.627524	9.216565	0.589041
p_4 (cm)	0	-2.935484	2.935484
p_5 (cm)	0	0.313918	0.313918
p_6 (cm)	0	1.936742	1.936742

Table G-2. Nominal and optimum right knee joint parameters for second one-half-cycle experimental marker data.

Right Knee Joint Parameter	Nominal	Optimized	Improvement
p_1 (°)	0	7.216444	7.216444
p_2 (°)	0	12.986174	12.986174
p_3 (°)	-4.070601	-0.228411	3.842190
p_4 (°)	1.541414	10.970612	9.429198
p_5 (cm)	0	-1.300621	1.300621
p_6 (cm)	-39.211319	-38.785646	0.425673
p_7 (cm)	0	-1.190227	1.190227
p_8 (cm)	0	-0.130610	0.130610
p_9 (cm)	0	1.293016	1.293016

Table G-3. Nominal and optimum right ankle joint parameters for second one-half-cycle experimental marker data.

Right Ankle Joint Parameter	Nominal	Optimized	Improvement
p_1 (°)	8.814964	31.399921	22.584957
p_2 (°)	0	1.211118	1.21112
p_3 (°)	26.890791	51.518589	24.627798
p_4 (°)	23	26.945919	3.945919
p_5 (°)	42	45.021534	3.021534
p_6 (cm)	0	-3.971358	3.971358
p_7 (cm)	-41.131554	-36.976040	4.155514
p_8 (cm)	0	-0.154441	0.154441
p_9 (cm)	-1	-3.345873	2.345873
p_{10} (cm)	9.113839	7.552444	1.561395
p_{11} (cm)	3.900829	7.561219	3.660390
p_{12} (cm)	1.116905	1.108033	0.008872

APPENDIX H
OPTIMUM JOINT PARAMETERS FOR MULTI-CYCLE & FIRST ONE-HALF-CYCLE EXPERIMENTAL MARKER DATA

Table H-1. Optimum right hip joint parameters for multi-cycle and first one-half-cycle experimental marker data.

Right Hip Joint Parameter	Multi-Cycle Optimized	First-Half-Cycle Optimized	Difference
p_1 (cm)	-7.518819	-7.377948	0.140871
p_2 (cm)	-9.268741	-9.257734	0.011007
p_3 (cm)	8.857706	8.124560	0.733146
p_4 (cm)	-2.123433	-2.050133	0.073300
p_5 (cm)	0.814089	0.813034	0.001055
p_6 (cm)	1.438188	0.656323	0.781865

Table H-2. Optimum right knee joint parameters for multi-cycle and first one-half-cycle experimental marker data.

Right Knee Joint Parameter	Multi-Cycle Optimized	First-Half-Cycle Optimized	Difference
p_1 (°)	-0.586205	7.621903	8.208108
p_2 (°)	14.854951	12.823259	2.031692
p_3 (°)	-2.724374	-0.642569	2.081805
p_4 (°)	2.404475	11.252668	8.848193
p_5 (cm)	-1.422101	-1.217316	0.204785
p_6 (cm)	-39.611720	-38.611100	1.000620
p_7 (cm)	-0.250043	-1.252732	1.002689
p_8 (cm)	-0.457104	-0.003903	0.453201
p_9 (cm)	1.471656	1.480035	0.008379

Table H-3. Optimum right ankle joint parameters for multi-cycle and first one-half-cycle experimental marker data.

Right Ankle Joint Parameter	Multi-Cycle Optimized	First-Half-Cycle Optimized	Difference
p_1 (°)	16.640499	-15.959751	32.600250
p_2 (°)	9.543288	-4.522393	14.065681
p_3 (°)	27.359342	18.986137	8.373205
p_4 (°)	13.197304	28.588479	15.391175
p_5 (°)	45.259512	36.840527	8.418985
p_6 (cm)	1.650689	3.624386	1.973697
p_7 (cm)	-41.185800	-43.537980	2.352180
p_8 (cm)	-1.510034	-3.370814	1.860780
p_9 (cm)	-2.141939	-2.246233	0.104294
p_{10} (cm)	11.244080	12.155750	0.911670
p_{11} (cm)	3.851262	0.488739	3.362523
p_{12} (cm)	0.283095	-1.207070	1.490165

APPENDIX I
OPTIMUM JOINT PARAMETERS FOR MULTI-CYCLE & SECOND ONE-HALF-CYCLE EXPERIMENTAL MARKER DATA

Table I-1. Optimum right hip joint parameters for multi-cycle and second one-half-cycle experimental marker data.

Right Hip Joint Parameter	Multi-Cycle Optimized	Second-Half-Cycle Optimized	Difference
p_1 (cm)	-7.518819	-7.884120	0.365301
p_2 (cm)	-9.268741	-10.160573	0.891832
p_3 (cm)	8.857706	9.216565	0.358859
p_4 (cm)	-2.123433	-2.935484	0.812051
p_5 (cm)	0.814089	0.313918	0.500171
p_6 (cm)	1.438188	1.936742	0.498554

Table I-2. Optimum right knee joint parameters for multi-cycle and second one-half-cycle experimental marker data.

Right Knee Joint Parameter	Multi-Cycle Optimized	Second-Half-Cycle Optimized	Difference
p_1 (°)	-0.586205	7.216444	7.802649
p_2 (°)	14.854951	12.986174	1.868777
p_3 (°)	-2.724374	-0.228411	2.495963
p_4 (°)	2.404475	10.970612	8.566137
p_5 (cm)	-1.422101	-1.300621	0.121480
p_6 (cm)	-39.611720	-38.785646	0.826074
p_7 (cm)	-0.250043	-1.190227	0.940184
p_8 (cm)	-0.457104	-0.130610	0.326494
p_9 (cm)	1.471656	1.293016	0.178640

Table I-3. Optimum right ankle joint parameters for multi-cycle and second one-half-cycle experimental marker data.

Right Ankle Joint Parameter	Multi-Cycle Optimized	Second-Half-Cycle Optimized	Difference
p_1 (°)	16.640499	31.399921	14.759422
p_2 (°)	9.543288	1.211118	8.332170
p_3 (°)	27.359342	51.518589	24.159247
p_4 (°)	13.197304	26.945919	13.748615
p_5 (°)	45.259512	45.021534	0.237978
p_6 (cm)	1.650689	-3.971358	5.622047
p_7 (cm)	-41.185800	-36.976040	4.209760
p_8 (cm)	-1.510034	-0.154441	1.355593
p_9 (cm)	-2.141939	-3.345873	1.203934
p_{10} (cm)	11.244080	7.552444	3.691636
p_{11} (cm)	3.851262	7.561219	3.709957
p_{12} (cm)	0.283095	1.108033	0.824938

LIST OF REFERENCES

Andriacchi, T.P., 1994. "Dynamics of Knee Malalignment." *Orthopedic Clinics of North America*, Volume 25, Number 3, Pages 395-403.

Andriacchi, T.P. and Strickland, A.B., 1985. "Gait Analysis as a Tool to Assess Joint Kinetics." In: Berme, N., Engin, A.E., Correia da Silva, K.M. (Editors), *Biomechanics of Normal and Pathological Human Articulating Joints*. Martinus Nijhoff Publishers, Dordrecht, The Netherlands, Pages 83-102.

Arnold, A.S, Asakawa, D.J, and Delp, S.L., 2000. "Do the Hamstrings and Adductors Contribute to Excessive Internal Rotation of the Hip in Persons with Cerebral Palsy?" *Gait & Posture*, Volume 11, Number 3, Pages 181-190.

Arnold, A.S. and Delp, S.L., 2001. "Rotational Moment Arms of the Hamstrings and Adductors Vary with Femoral Geometry and Limb Position: Implications for the Treatment of Internally-Rotated Gait." *Journal of Biomechanics*, Volume 34, Number 4, Pages 437-447.

Bell, A.L., Pedersen, D.R., and Brand, R.A., 1990. "A Comparison of the Accuracy of Several Hip Center Location Prediction Methods." *Journal of Biomechanics*, Volume 23, Number 6, Pages 617-621.

Blankevoort, L., Huiskes, A., and de Lange, A., 1988. "The Envelope of Passive Knee-Joint Motion." *Journal of Biomechanics*, Volume 21, Number 9, Pages 705-720.

Bogert, A.J. van den, Smith, G.D., and Nigg, B.M., 1994. "In Vivo Determination of the Anatomical Axes of the Ankle Joint Complex: An Optimization Approach." *Journal of Biomechanics*, Volume 27, Number 12, Pages 1477-1488.

Bryan, J.M., Hurwitz, D.E., Bach, B.R., Bittar, T., and Andriacchi, T.P., 1997. "A Predictive Model of Outcome in High Tibial Osteotomy." In *Proceedings of the 43rd Annual Meeting of the Orthopaedic Research Society*, San Francisco, California, February 9-13, Volume 22, Paper 718.

Cappozzo, A., Catani, F., and Leardini, A., 1993. "Skin Movement Artifacts in Human Movement Photogrammetry." In *Proceedings of the XIVth Congress of the International Society of Biomechanics*, Paris, France, July 4-8, Pages 238-239.

Cappozzo, A., Leo, T., and Pedotti, A., 1975. "A General Computing Method for the Analysis of Human Locomotion." *Journal of Biomechanics*, Volume 8, Number 5, Pages 307-320.

CDC, 2003. *Targeting Arthritis: The Nation's Leading Cause of Disability*. Centers for Disease Control and Prevention, National Center for Chronic Disease Prevention and Health Promotion, Atlanta, Georgia. Accessed: http://www.cdc.gov/nccdphp/aag/pdf/aag_arthritis2003.pdf, February, 2003.

Challis, J.H. and Kerwin, D.G., 1996. "Quantification of the Uncertainties in Resultant Joint Moments Computed in a Dynamic Activity." *Journal of Sports Sciences*, Volume 14, Number 3, Pages 219-231.

Chao, E.Y. and Sim, F.H., 1995. "Computer-Aided Pre-Operative Planning in Knee Osteotomy." *Iowa Orthopedic Journal*, Volume 15, Pages 4-18.

Chao, E.Y.S., Lynch, J.D., and Vanderploeg, M.J., 1993. "Simulation and Animation of Musculoskeletal Joint System. *Journal of Biomechanical Engineering*, Volume 115, Number 4, Pages 562-568.

Churchill, D.L., Incavo, S.J., Johnson, C.C., and Beynnon, B.D., 1998. "The Transepicondylar Axis Approximates the Optimal Flexion Axis of the Knee." *Clinical Orthopaedics and Related Research*, Volume 356, Number 1, Pages 111-118.

Chéze, L., Fregly, B.J., and Dimnet, J., 1995. "A Solidification Procedure to Facilitate Kinematic Analyses Based on Video System Data." *Journal of Biomechanics*, Volume 28, Number 7, Pages 879-884.

Davis, B.L., 1992. "Uncertainty in Calculating Joint Moments During Gait." In *Proceedings of the 8th Meeting of European Society of Biomechanics*, Rome, Italy, June 21-24, Page 276.

de Leva, P., 1996. "Adjustments to Zatsiorsky-Seluyanov's Segment Inertia Parameters." *Journal of Biomechanics*, Volume 29, Number 9, Pages 1223-1230.

Delp, S.L., Arnold, A.S., and Piazza, S.J., 1998. "Graphics-Based Modeling and Analysis of Gait Abnormalities." *Bio-Medical Materials and Engineering*, Volume 8, Number 3/4, Pages 227-240.

Delp, S.L., Arnold, A.S., Speers, R.A., and Moore, C.A., 1996. "Hamstrings and Psoas Lengths During Normal and Crouch Gait: Implications for Muscle-Tendon Surgery." *Journal of Orthopaedic Research*, Volume 14, Number 1, Pages 144-151.

Delp, S.L., Loan, J.P., Hoy, M.G., Zajac, F.E., Topp, E.L., and Rosen, J.M., 1990. "An Interactive Graphics-Based Model of the Lower Extremity to Study Orthopaedic Surgical Procedures." *IEEE Transactions on Biomedical Engineering*, Volume 37, Number 8, Pages 757-767.

Heck, D.A., Melfi, C.A., Mamlin, L.A., Katz, B.P., Arthur, D.S., Dittus, R.S., and Freund, D.A., 1998. "Revision Rates Following Knee Replacement in the United States." *Medical Care*, Volume 36, Number 5, Pages 661-689.

Holden, J.P. and Stanhope, S.J., 1998. "The Effect of Variation in Knee Center Location Estimates on Net Knee Joint Moments." *Gait & Posture*, Volume 7, Number 1, Pages 1-6.

Holden, J.P. and Stanhope, S.J., 2000. "The Effect of Uncertainty in Hip Center Location Estimates on Hip Joint Moments During Walking at Different Speeds." *Gait & Posture*, Volume 11, Number 2, Pages 120-121.

Hollister, A.M., Jatana, S., Singh, A.K., Sullivan, W.W., and Lupichuk, A.G., 1993. "The Axes of Rotation of the Knee." *Clinical Orthopaedics and Related Research*, Volume 290, Number 1, Pages 259-268.

Hurwitz, D.E., Sumner, D.R., Andriacchi, T.P., and Sugar, D.A., 1998. "Dynamic Knee Loads During Gait Predict Proximal Tibial Bone Distribution." *Journal of Biomechanics*, Volume 31, Number 5, Pages 423-430.

Inman, V.T., 1976. "The Joints of the Ankle." Williams and Wilkins Company, Baltimore, Maryland.

Kennedy, J. and Eberhart, R.C., 1995. "Particle Swarm Optimization." In *Proceedings of the 1995 IEEE International Conference on Neural Networks*, Perth, Australia, November 27 - December 1, Volume 4, Pages 1942-1948.

Lane, G.J., Hozack, W.J., Shah, S., Rothman, R.H., Booth, R.E. Jr., Eng, K., Smith, P., 1997. "Simultaneous Bilateral Versus Unilateral Total Knee Arthroplasty. Outcomes Analysis." *Clinical Orthopaedics and Related Research*, Volume 345, Number 1, Pages 106-112.

Leardini, A., Cappozzo, A., Catani, F., Toksvig-Larsen, S., Petitto, A., Sforza, V., Cassanelli, G., and Giannini, S., 1999. "Validation of a Functional Method for the Estimation of Hip Joint Centre Location." *Journal of Biomechanics*, Volume 32, Number 1, Pages 99-103.

Lu, T.-W. and O'Connor, J.J., 1999. "Bone Position Estimation from Skin Marker Coordinates Using Global Optimisation with Joint Constraints." *Journal of Biomechanics*, Volume 32, Number 2, Pages 129-134.

Pandy, M.G., 2001. "Computer Modeling and Simulation of Human Movement." *Annual Reviews in Biomedical Engineering*, Volume 3, Number 1, Pages 245-273.

Piazza, S.J., Okita, N., and Cavanagh, P.R., 2001. "Accuracy of the Functional Method of Hip Joint Center Location: Effects of Limited Motion and Varied Implementation." *Journal of Biomechanics*, Volume 34, Number 7, Pages 967-973.

Prodromos, C.C., Andriacchi, T.P., and Galante, J.O., 1985. "A Relationship Between Gait and Clinical Changes Following High Tibial Osteotomy." *Journal of Bone Joint Surgery (American)*, Volume 67, Number 8, Pages 1188-1194.

Rahman, H., Fregly, B.J., and Banks, S.A., 2003. "Accurate Measurement of Three-Dimensional Natural Knee Kinematics Using Single-Plane Fluoroscopy." In *Proceedings of the 2003 Summer Bionengineering Conference*, The American Society of Mechanical Engineers, Key Biscayne, Florida, June 25-29.

Schutte, J.F., Koh, B., Reinbolt, J.A., Haftka, R.T., George, A.D., and Fregly, B.J., 2003. "Scale-Independent Biomechanical Optimization." In *Proceedings of the 2003 Summer Bioengineering Conference*, The American Society of Mechanical Engineers, Key Biscayne, Florida, June 25-29.

Sommer III, H.J. and Miller, N.R., 1980. "A Technique for Kinematic Modeling of Anatomical Joints." *Journal of Biomechanical Engineering*, Volume 102, Number 4, Pages 311-317.

Stagni, R., Leardini, A., Benedetti, M.G., Cappozzo, A., and Cappello, A., 2000. "Effects of Hip Joint Centre Mislocation on Gait Analysis Results." *Journal of Biomechanics*, Volume 33, Number 11, Pages 1479-1487.

Tetsworth, K. and Paley, D., 1994. "Accuracy of Correction of Complex Lower-Extremity Deformities by the Ilizarov Method." *Clinical Orthopaedics and Related Research*, Volume 301, Number 1, Pages 102-110.

Vaughan, C.L., Davis, B.L., and O'Connor, J.C., 1992. *Dynamics of Human Gait*. Human Kinetics Publishers, Champaign, Illinois, Page 26.

Wang, J.-W., Kuo, K.N., Andriacchi, T.P., and Galante, J.O., 1990. "The Influence of Walking Mechanics and Time on the Results of Proximal Tibial Osteotomy." *Journal of Bone and Joint Surgery* (American), Volume 72, Number 6, Pages 905-913.

BIOGRAPHICAL SKETCH

Jeffrey A. Reinbolt was born on May 6, 1974 in Bradenton, Florida. His parents are Charles and Joan Reinbolt. He has an older brother, Douglas, and an older sister, Melissa. In 1992, Jeff graduated salutatorian from Southeast High School, Bradenton, Florida. After completing his secondary education, he enrolled at the University of Florida supported by the Florida Undergraduate Scholarship and full-time employment at a local business. He earned a traditional 5-year engineering degree in only 4 years. In 1996, Jeff graduated with honors receiving a Bachelor of Science degree in engineering science with a concentration in biomedical engineering. He used this foundation to assist in the medical device development and clinical research programs of Computer Motion, Inc., Santa Barbara, California. In this role, Jeff was Clinical Development Site Manager for the Southeastern United States and he traveled extensively throughout the United States, Europe, and Asia collaborating with surgeons and fellow medical researchers. In 1998, Jeff married Karen, a student he met during his undergraduate studies. After more than 4 years in the medical device industry, he decided to continue his academic career at the University of Florida. In 2001, Jeff began his graduate studies in Biomedical Engineering and he was appointed a graduate research assistantship in the Computational Biomechanics Laboratory. He plans to continue his graduate education and research activities through the pursuit of a Doctor of Philosophy in mechanical engineering. Jeff would like to further his creative involvement in problem solving and the design of solutions to overcome healthcare challenges.